

Coarse-grained DNA model capable of simulating ribose flexibility

N.A. Kovaleva,^{1, a)} I.P. Koroleva (Kikot),¹ M.A. Mazo,¹ and E.A. Zubova^{1, b)}

N.N. Semenov Institute of Chemical Physics, Russian Academy of Sciences,

4 Kosygin Street, Moscow 119991, Russia

(Dated: 27 April 2019)

We propose a "sugar" coarse-grained (CG) DNA model capable of simulating both biologically significant B- and A-DNA. The model also demonstrates both the A to B and the B to A transitions. The number of degrees of freedom is reduced to six grains per nucleotide. We show that this is the minimal number sufficient for this purpose. The key features of the model are (1) simulation of sugar repuckering between C2'-endo and C3'-endo by the use of one nonharmonic potential and one three-particle potential, (2) explicit representation of ions in solution around the DNA, (3) implicit solvent approach and (4) sequence dependence. We obtain parameters of the model from the all atom AMBER force field. The model can be used to study large local deformations of long DNA molecules (for example, in binding with proteins). Small modification of the model can provide the possibility of modeling base pairs openings in melting, transcription and replication. And one can also simulate the interactions of the DNA molecule with different types of ions in different kinds of solutions.

Keywords: DNA; coarse graining; ribose; polymorphism

I. INTRODUCTION

Local DNA flexibility is crucial for its biological function. The deformation of the double helix is achieved through three types of mobility in the DNA backbone: concerted rotations around α and γ^1 , ζ and ε^2 torsions, and ribose flexibility. The last mentioned type makes the main contribution into providing the observed DNA flexibility.

The local sugar repuckerings are very common in physiological saline. In vivo, they take place in binding of proteins (such as TBP, SRY, LEF-1, PurR) to the minor groove of B-DNA. During this process the minor groove widens through several sugar repuckerings into A-like conformations³. Many local B to A conversions have been observed in protein and drug-bound DNA crystal complexes⁴. Particularly, such conversion takes place when an enzyme interacts with the atoms ordinarily buried within the backbone (O3', for example). A-DNA is more resistant to ultraviolet radiation, therefore DNA undergoes a transition from B to A in Gram-positive bacteria during sporulation⁵.

One can obtain DNA crystals from a solution in both the A- and B-forms depending on salt concentration, relative humidity and base pairs sequence (for a review, see, for example,⁶ and references therein). In a solution, one can induce a B to A transition by increasing salt concentration and/or adding ethanol to the solvent^{7,8}. The ethanol concentration, at which the B to A transition occurs, depends on the nucleotide sequence⁹: more C:G pairs shift the transition to smaller ethanol concentrations. It should be noted that other characteristics of a DNA nucleotide (both structural and dynamical ones) also depend on its base and a few neighboring bases.

Therefore, the geometry (and, as a consequence, mechanical and dynamical properties) of both the A-DNA and B-DNA forms is a result of a complex balance of interdependent factors: torsion and valence angles in the backbone; sugar puckers; sequence dependent base pair stacking; electrostatic interactions of DNA with solvent molecules and with salt ions. From the physical point of view, the understanding of this balance is equivalent to the construction of a coarse-grained (CG) DNA model able to reproduce key features of the DNA behavior.

The last ten years witnessed the extensive development of CG models for different substances¹⁰, particularly for large biomolecules¹¹. Regular methods for obtaining CG force fields from the all-atom ones have been developed. However, all the regular methods imply that all potentials are pairwise and have a certain simple form. As we will show later, if the objective is to model the effect of ribose flexibility on DNA geometry, one has to use at least one three-particle potential.

In many works, DNA behaviour is simulated within the framework of CG models with phenomenologically chosen parameters (for a review, see, for example,¹²). The model with the coarsest grain (consisting of two complementary nucleotides), the worm-like chain model, can reproduce the simplest macro-mechanical properties which are common for DNA and the other semiflexible polymers. A modification of this model¹³ allows one to obtain both bending and torsional persistent lengths (consistent with experiments). However, the modified model does not provide the correct value for the relaxation rate of bending fluctuations, because the DNA bending proves to be highly anharmonic. Another approach with similar "coarseness" is the representation of DNA as a stack of interacting plane bases¹⁴. To simulate DNA melting, one needs a model with finer grain, at least one grain for every nucleotide¹⁵. However, this scale still does not allow to take into account even the simplest geometrical nonlinearity of DNA strands. The next step is to divide

^{a)}Electronic mail: natkov@polymer.chph.ras.ru

^{b)}Electronic mail: zubova@chph.ras.ru

a nucleotide into 3 grains: phosphate, ribose and nucleic base¹⁶. On this scale, it is already possible to fit helical parameters either for B-form or for A-form (not for both) by tuning the lengths, angles and rigidities¹⁷. The next approximation to the double helix structure is a pair of zigzag chains with interacting plane nucleobases (that is two grains and one solid body or, equivalently, five grains per nucleotide)¹⁸. However, this model still can not reproduce the ribose flexibility. We will show that for this purpose one needs at least 3 grains and one solid body (or, equivalently, six grains) per nucleotide, one nonlinear potential, and, in addition, explicit modeling of ions.

Here, we present a minimal CG model of the DNA molecule which can reproduce ribose flexibility, and, correspondingly, both A-DNA and B-DNA forms. On the basis of experimental and theoretical (MD simulations within the framework of an all atom model) data, we analyze the mobility of the DNA double helix, unite atomic groups into grains and choose the potentials of interaction. Besides backbone interactions in strands, we define the minimal adequate solvent model which enables to simulate A-DNA.

The approach we use in this work has been originally formulated in¹⁹. There, the choice of grains and potentials for simulating ribose flexibility has been described. In work²⁰ the B-DNA form has been modeled in the framework of this approach, but without implementation of ribose flexibility and with implicit solvent (generalized Born approximation with the Debye-Huckel correction for salt effects²¹). In the framework of this version, DNA heat conductivity was estimated²² and DNA stretching was investigated²³. However, this version is admissible only when one may neglect the ribose flexibility (under low temperatures or when the molecule can be extended but not bent and not compressed). At temperature 300 K, the behaviour of this CG B-DNA and the all atom AMBER model significantly differ²⁰. In the present work we suggest a realization of the model (hereinafter referred to as the "sugar" CG DNA model) which adequately describes ribose flexibility and interactions between negative charges on DNA and explicit ions in implicitly treated solvent. This realization of the model is capable of simulating both A- and B-DNA forms under corresponding conditions.

II. CONSTRUCTION OF THE SUGAR CG DNA MODEL

As a basis for the CG model construction, we accept the AMBER force field²⁴ for base pairs interactions. This choice is justifiable, considering that the empirical force fields reproduce the interactions between bases best²⁵. We analyze the DNA dynamics in solvents at 300 K in the framework of the all-atom AMBER model, as well as the geometric changes of the DNA helix in A-B transition and base-pair opening. On the basis of these data, we divide the DNA chains into grains and find the potentials for interactions between the grains. Finally, we choose the

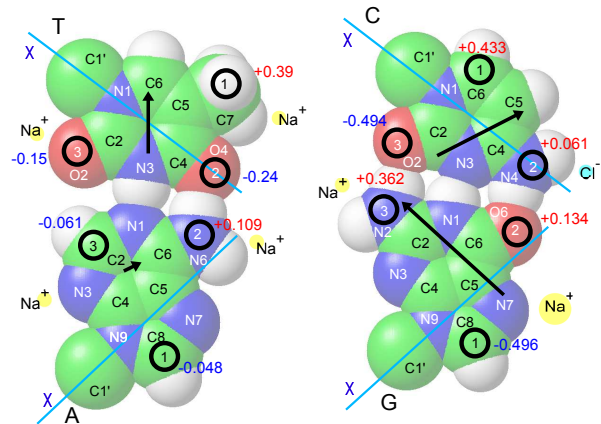


FIG. 1. Coarse-graining of the natural base pairs (A:T and G:C). We show the locations and the charges of three rigidly bound grains modeling every base. The rotation axes (glycosidic bonds χ with the sugar rings) are marked. DNA atoms are designated according to²⁶, and we depict their van-der-Waals radii. The black arrows present electric dipole moments of the bases (according to the charge distribution in AMBER), and the circles near atoms of the bases - zones around A-DNA where one can find ions Na^+ or Cl^- with maximal probability²⁷.

description of the medium: the models for the ions and the solvent.

A. Base stacking and base pairing

We model a base as three rigidly bound grains which can rotate around an axis coinciding with the real rotation axis of the base: the glycosidic bond χ . We placed the grains on some (heavy) atoms of the bases (see fig. 1). One of the atoms was chosen on one side of the rotation axis, the two others - on the other side, at maximum distance from the center of the base. The objective of this choice was to best approximate the real moments of inertia of the base.

For base A (Adenine) we placed the grains on atoms C8, N6, C2; for base T (Thymine) - on atoms C7, O4, O2; for base G (Guanine) - on atoms C8, O6, N2; and for base C (Cytosine) - on atoms C6, N4, O2 (see fig. 1).

Masses of grains m_1, m_2, m_3 on a base X ($X = A, T, G, C$) were found from the two conditions: (1) equality of the total mass of the grains to the mass of the base ($m_1 + m_2 + m_3 = m_X$) and (2) coincidence of the mass centers of the three grains and the base. Numerical values for masses of grains and moments of inertia of the CG and real bases are given in table I.

Knowing the coordinates of the three grains, one can find the coordinates of all the base atoms and compute the energy of base pairing and base stacking as the sum of pairwise atomic electrostatic and van-der-Waals inter-

TABLE I. Masses of grains m_1 , m_2 , m_3 and moments of inertia of the real i_{xx} and i_{yy} and the CG I_{xx} and I_{yy} bases A, T, G, C. Masses of the grains are given in a.e.m., the moments of inertia - in a.e.m. $\cdot\text{\AA}^2$.

X	m_1	m_2	m_3	i_{xx}	I_{xx}	i_{yy}	I_{yy}
A	52.230	28.139	53.632	690	475	1704	1712
T	51.822	16.204	56.974	584	256	1636	1543
G	61.731	34.357	53.912	1302	800	1885	1858
C	39.254	35.492	35.254	233	164	1344	1231

actions. For them, we used the AMBER force field²⁴. In articles²² and²³, where only the B-DNA was simulated, the partial interaction between bases was used to decrease the computation time. In the present realization of the model every atom of a base interacts with every atom of the complementary base and with all the atoms of two neighboring base pairs. It allows to simulate the A-DNA form and other deformed structures (for example, base pair opening).

The accepted interactions between bases are computationally expensive (as compared to the other interactions in the CG model). We used them only as a foundation to construct the adequate CG backbone and test the obtained structure. If one uses the sugar CG model in long simulations of biological processes in the future, the described scheme is the first thing one would want to change.

B. Choice of grains for backbone: C1', P, C3'

We choose the locations of all the grains on (heavy) atoms. The main principle was: one may distort the mass distribution of the molecule, but one preserves its key geometric nodes. Let us show that we will need three grains per nucleotide for the backbone (see fig. 2).

The first grain was chosen on atom C1' because it is the point of suspension of the base, and the rotation axis of the base (glycosidic bond) passes through this atom. Crystallographic data²⁸ show that bases rotate around this axis considerably, while valence angles O4'C1'N1(N9) and C2'C1'N1(N9) practically do not change and fix the direction of the glycosidic bond relative to the ribose ring. This is the key geometric peculiarity of the connection between a base and the backbone, and we keep this peculiarity in our model.

The second grain was chosen on phosphorus atom, and united phosphate group and three atoms (C5', H5'1, H5'2) which normally move together with the phosphate²⁹. As we want to minimize the number of grains per nucleotide, we would tend to restrict the backbone to the chain (...-P-C1'-P-C1'-...). However, all atom MD simulations show that the presence of the very flexible sugar rings between the atoms P and C1' allows the "torsion" angles in this chain to vary over a very wide range, while the "torsion" angles in the chain (...-P-P-P-...) keep their mean values quite satisfactorily. To

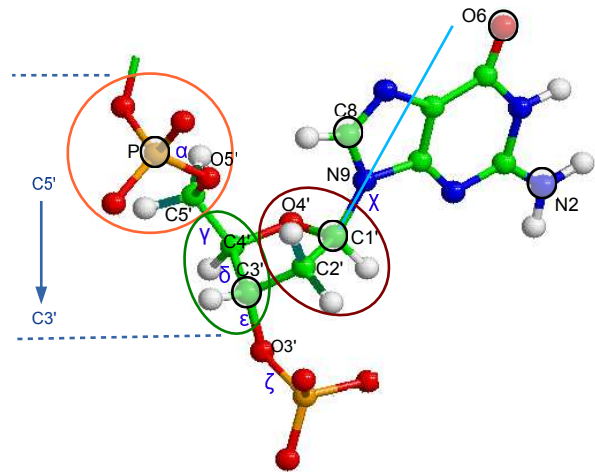


FIG. 2. Coarse-graining of the sugar-phosphate backbone. We show locations of the grains and (for the backbone) groups of atoms united into the grains. Notations for atoms and torsion angles are from²⁶. A nucleobase rotates about the glycosidic bond χ .

preserve this feature, we need at least one more grain per nucleotide.

Besides, we would like to build a backbone which can serve as a support for the moving bases at their opening and in A-B transition (which is the case for the real sugar-phosphate backbone of DNA). This purpose is also not achieved for the chain (...-P-C1'-P-C1'-...) as the atoms C1' always move together with the bases.

When a sugar repuckers, the torsion angles around the bonds adjoining the sugar ring also change, and so does the position of the ring relative to the two neighboring phosphate groups as well as the distance between the groups. The adjacent base pairs move relative to each other, and the local geometry changes from B-like to A-like (see fig.3). One can see that the atom C4' moves with the sugar ring in sugar repuckering. On the contrary, the displacement of the atom C3' is mostly caused by the necessity to change the geometric form of the chain of phosphates. Therefore, we choose the third grain on the atom C3'.

As a result, to hold the needed form of the DNA strand, we use "valence" bonds, and "valence" and "torsion" angles in the chain of grains (...-P-C3'-P-C3'-...). To model the ribose flexibility, we add grains C1' (connected to bases) attached to the C3' grains of this chain. The position of the bond C3'-C1' relative to the chain (...-P-C3'-P-C3'-...) should have two locations divided by a barrier - which reflects two main states of the ribose.

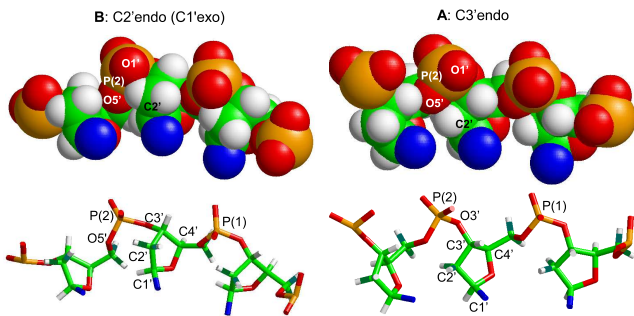


FIG. 3. Position of a sugar ring relative to the chain of phosphorus atoms in B- and A-DNA forms (GLACTONE³⁰). The valence bonds and angles, on the one hand, and the van-der-Waals interactions, on the other hand, provide two stable positions of the ring relative to the phosphates exactly when the ring has C2'-endo (B-DNA) and C3'-endo (A-DNA) puckers: between two phosphates and under the chain of phosphates. Intermediate positions suffer strong steric hindrance, which results in a barrier between these two energy minima. When the ring changes its conformation, it has to change its position relative to the chain of phosphates (distance C1'P2). This, in turn, has to change the distance between the phosphates. So we have correlations: (C2'-endo \Leftrightarrow small |C1'P2| \Leftrightarrow large |P1 P2| \Leftrightarrow B-DNA) and (C3'-endo \Leftrightarrow large |C1'P2| \Leftrightarrow small |P1 P2| \Leftrightarrow A-DNA).

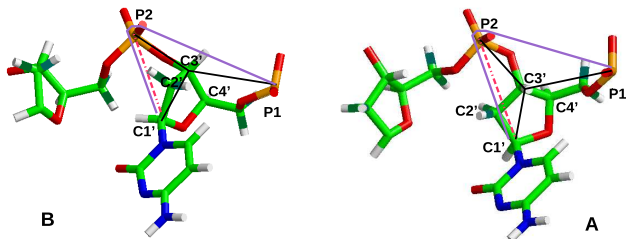


FIG. 4. CG model of sugar repuckering from C2'-endo (B-DNA) to C3'-endo (A-DNA). We show the pyramid {P1 P2 C3' C1'} composed of grains of the sugar CG model in B-DNA and A-DNA forms (GLACTONE³⁰). For the bonds C3'-P2, P1-C3' and C3'-C1' we choose sufficiently rigid harmonic potentials. For the bond C1'-P2, we introduce a double-well potential. The two wells correspond to two main sugar pucker (see fig. 3). The correlation of the distance |P1 P2| with |C1' P2| is described by potential (1). This potential can be symbolically depicted as one spring thrown from grain P1 to grain C1' over grain P2. For the long bond P1-C1', we use a soft spring.

C. CG simulation of ribose flexibility: choice of potentials for pyramid {P1 P2 C3' C1'}

Ribose flexibility causes deformations of the CG pyramid {P1 P2 C3' C1'} (see fig. 4) and is modeled through double-well potential for bond C1'-P2. As we saw (fig. 3), one also needs correlation between the distances |P1 P2| and |C1' P2|, which we introduce through three-particle

potential

$$U = \frac{1}{2}k_P(|P(1)P(2)| + t_P|C1'P(2)| - l_{P0})^2, \quad (1)$$

where $t_P > 0$.

From direct geometric considerations, one could also expect a (positive) correlation between distances |P1C1'| and |C1'P2|. However, as we will see from the all-atom simulations (chapter IID 2), one can use a soft harmonic potential for this bond: the distance |P1 C1'| does not correlate with the sugar pucker. Indeed, there are five valence bonds and three torsion angles between atoms P1 and C1', and these degrees of freedom are only weakly connected with sugar repuckering.

D. Obtaining parameters of CG potentials from the all-atom AMBER model

In spite of the problems in simulation with large ethanol or salt concentrations, one can consider empirical force fields AMBER and CHARMM as providing sufficiently reliable balance of interactions in the DNA molecule in water with both small (³¹, B-DNA) and high (³² and ³³, B-A transition) salt concentrations, which allows to lean upon these all-atom models in construction of CG models.

For coarse-graining, we used two methods. First, to obtain rigidities of some "valence" bonds, "valence" and "torsion" angles in our CG model, we used the simplest Boltzmann inversion method³⁴ for all-atom MD trajectories of Dickerson-Drew dodecamer (the sequence 5'-CGCGAATTCGCG-3' on the first chain and, correspondingly, 3'-GCGCTTAAGCGC-5' on the other; in the following, the number of a nucleotide is its serial number in counting first along the first chain from 5' to 3' and then along the second chain from 5' to 3'). More exactly, we analyzed the behavior of a B-DNA in water (AMBER, parmbsc0³⁵) and an A-DNA in the mixture of ethanol and water (85:15) (AMBER, parm99²⁴). We supposed that the bonds and angles under consideration have Boltzmann distribution $p(l) \sim \exp(-U(l)/kT)$, where U is a harmonic function: $U(l) = \frac{1}{2}K_l(l - l_0)^2$ ($U(\theta) = \frac{1}{2}K_\theta(\theta - \theta_0)^2$). For every nucleotide, we made a frequency histogram for every relevant distance and angle. Then we approximated the histogram by Gaussian distribution or by the sum of two Gaussian distributions, and determined their means (centers) and standard deviations. Finally, we took the averages of the centers and of the deviations over the nucleotides. We believed that so obtained distances l_0 (angles θ_0) and rigidities K_l (K_θ) can be regarded as estimates of mean values and effective rigidities for bonds and angles in our CG model.

Let us notice that, in this approach, the obtained rigidities take into account not only the (valence, torsion and van-der-Waals) interactions between DNA atoms, together with DNA solvation. In addition, these rigidities

partly "include" several interactions which we plan to introduce separately: base stacking; electrostatic interactions between charges on DNA, and between charges on DNA and ions. Therefore, to verify the obtained rigidities and, in some cases, to evaluate the potentials which can not be derived in such a way (for example, in the case of the double-well potential for the bond C1'-P2), we used another method (method of "relaxation").

Namely, to obtain the energy of interaction between two grains at a given distance, we took an all-atom fragment of one DNA strand (without charges, in vacuum) between the atoms corresponding to these grains, and located these atoms at the needed distance one from another. Then we minimized the energy of the system (in the framework of the AMBER force field) as a function of coordinates of all the rest atoms (and so we carried out the "relaxation" of the system). The obtained value of energy was regarded as the energy of interaction between the grains at this distance. Changing the distance between the grains, we got the dependence of the energy on the distance. In this way one can evaluate potentials of "valence" bonds in a CG model.

The details of the estimations of the mean values and rigidities for the bonds and angles of the CG model are collected in Appendix A (section VII). In the rest of this section, we shortly list the most important results.

1. "Valence" bonds C3'-C1', C3'-P(2) and P(1)-C3'

The rigidities of the bonds C3'-C1' and C3'-P(2) (see fig. 5) are provided by valence bonds and angles (under tension) and by van-der-Waals forces (under compression), therefore the bonds C3'-C1' and C3'-P(2) are rigid. The bond P(1)-C3', consisting of four valence bonds, is softer. The frequency histograms obtained from MD trajectories for these bonds have one narrow peak for all the nucleotides. The estimates of the lengths and the rigidities made by different methods are listed in table VI of Appendix A (section VII).

2. Bonds P(1)-C1', C1'-P(2) and P(1)-P(2) in pyramid {P(1)P(2)C3'C1'} modeling sugar ring

In pyramid {P(1)P(2)C3'C1'} three bonds C3'-C1', C3'-P(2) and P(1)-C3' are rigid and we use for them harmonic potentials (see IID1), while the rest three bonds P(1)-C1', C1'-P(2), P(1)-P(2) are connected with the flexible sugar ring. As we expected from geometric considerations (see IIC), only the length C1'-P(2) unambiguously correlates with pseudorotation angle τ (see fig. 17 in Appendix A (section VII)). The length P(1)-P(2) demonstrates broad double-humped distribution not always connected with the sugar repuckering, and the length P(1)-C1' has large additional noise.

To estimate the double-well potential of the bond C1'-P(2), we used the method of "relaxation" (see the begin-

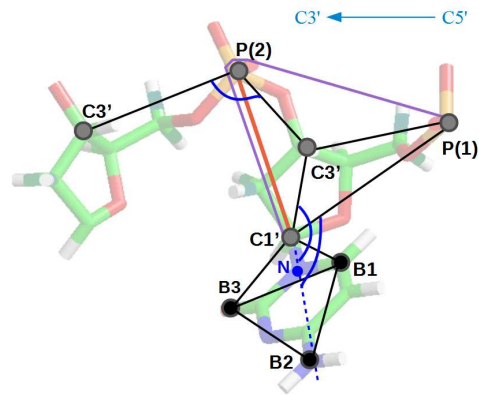


FIG. 5. "Valence" bonds and angles of the sugar CG model. The double-well bond C1'-P(2) models ribose flexibility, the length $|P(1)P(2)|$ correlates with the length $|C1'P(2)|$ (potential (1) is symbolically depicted as the poly-line P(1)-P(2)-C1'). Atom N (N1 or N9) does not belong to the grains of the CG model, it is shown merely to determine the direction of the glycosidic bond, which the base rotates around.

ning of section IID), because the depths of the wells and the height of the barrier can not be obtained from MD simulations. The derived potential proved to be double-well as we had expected, only the depths of the wells are different: B-minimum is lower (see fig. 18 in Appendix A (section VII)). The lengths and rigidities in both wells well agree with the estimates from the MD trajectory for A-DNA.

It is known³⁶ that the sugar pucker typical of B-DNA is energetically more favorable for all bases except cytosine. Estimates made by different methods give the energy difference in the interval 0.2-0.9 kcal/mol. For cytosine, the energy minimum corresponding to A-form is 0.3-0.5 kcal/mol lower than that of B-form. The energy barrier between these two main sugar puckers is about 2-4 kcal/mol (at temperature 25°C, $kT \approx 0.6$ kcal/mol).

Because the fragment of chain used in "relaxation" method did not have any base attached to it, one would expect the depths of the two wells to be equal one to another. But we see that the B-minimum is lower. In this connection, one can remember work³⁷, where, to provide in AMBER force field a spontaneous B to A transition in $d[CCAACGTTGG]_2$ sequence in 85% ethanol solution, the authors had to make "reduction of the V2 term in the O-C-C-O torsions from 1.0 to 0.30 kcal/mol to better stabilize the C3'-endo sugar pucker". We also found that the higher A-minimum obstructs formation of the A-DNA, requiring unrealistic potentials for interactions between ions. Therefore we chose the double-well potential for the bond C1'-P(2) with equal minima.

We calculated parameters t_P and l_{P0} of the three-particle potential (1) from conditions that the characteristic values for lengths $|P(1)P(2)|_A$ and $|C1'P(2)|_A$ obtained from MD simulation of A-DNA (see table VII)

have to correspond to zero of the potential; as well as the uncharacteristic values for these lengths (only for $|C1'P(2)|_B$ we chose, instead of the value 4.3\AA , the lesser amount 4.2\AA). The two equations give $t_P = 1.27$ and $l_{P0} = 12.235\text{\AA}$. Deviations of the values $|P(1)P(2)| + t_P |C1'P(2)| - l_{P0}$ from zero depend on the pseudorotational angle: in A-DNA, they are less in the "north"(A) region. Therefore the rigidity k_P in (1) can not be chosen uniquely. It may be estimated as $10\text{-}40 \text{ kcal}/(\text{mol}\cdot\text{\AA}^2)$ in A-DNA, while in "soft" B-DNA it is around $5 \text{ kcal}/(\text{mol}\cdot\text{\AA}^2)$. We used the amount $39 \text{ kcal}/(\text{mol}\cdot\text{\AA}^2)$ to provide better correlation between the lengths $|P(1)P(2)|$ and $|C1'P(2)|$.

For the bond $P(1)\text{-}C1'$, one can observe two peaks in histograms in both A- and B-DNA forms, but this is not connected with the ribose flexibility: the populations of the peaks are the same in both forms (see table VII in Appendix A, section VII), and from fig. 17 one can see that the correlation of this length with pseudorotational angle is small. Even where this correlation does exist, the changes of this length are comparable with its thermal fluctuations. This fact allows one not to introduce a three-particle potential of type (1) for this bond, but to restrict oneself to a soft harmonic potential with the rigidity close to the rigidity obtained from all-atom simulation.

3. "Valence" and "torsion" angles

In our CG model, every one of the two DNA strands is a sequence of pyramids $\{P(1)P(2)C3'C1'\}$ surrounding riboses. Every pyramid has two common vertices with two neighboring pyramids, and every pyramid can change its shape, which imitates ribose flexibility. In the all atom models the zigzag (...-C3'-P-C3'-P-...) keeps its shape sufficiently well. To govern the shape of this backbone, one has to introduce "valence" and "torsion" angles into it. These angles do not differ appreciably in the all atom MD simulations of A- and B-DNA forms (see table VIII in Appendix A, section VII), which confirms the adequacy of our choice of grains. So, we will consider the shape of the zigzag (...-C3'-P-C3'-P-...) to be universal: not depending on sugar puckers.

Contrary to the angles on the backbone, the "valence" angles responsible for the direction of the glycosidic bond relative to the backbone, as well as "torsion" angles for base pair opening and for rotation of base around the glycosidic bond differ considerably in crystallographic (GLACTONE³⁰) A- and B-DNA forms (see table IX in Appendix A, section VII). However, in MD trajectories, "torsion" angle $C1'C3'P(2)C3'$ for base pair opening around the "short" bond $C3'P(2)$ and the angle of rotation of base around the glycosidic bond $C3'C1'N(1,9)C(6,8)$ do not differ at all. In other cases we always chose the values corresponding to A-DNA.

One should also note, that the rigidity of the angle $C3'C1'N(1,9)C(6,8)$, obtained from the all atom trajec-

tories, has nothing to do with the real rigidity of this angle. Indeed, in one nucleotide, there is no steric hindrance for the rotation of a base, which means very small own rigidity of this angle. The obstacles to the rotation create the atoms of the neighboring bases. Therefore, in our CG model, the rigidity of this angle is chosen to be very small.

E. Modeling of DNA environment

It is clearly seen from the all atom modeling (see fig.1 in³⁸ and fig.7 in³¹) that most counter-ions are situated near the surface of A-DNA, and almost in one layer. Closer examination shows that the counter-ions are located mostly in the major groove of A-DNA both in ethanol-water mixture³⁷ and in a small water drop³². It allows the phosphates on the opposite sides of the major groove to approach each other, and thus the characteristic cavity of A-DNA forms. It is obvious that such ion distribution can not be described in the framework of any implicit approach. And, indeed, in work³⁹, where the generalized Born approximation with Debye-Huckel correction for salt effects was used, only some shift of the DNA form from B to A was reported when 1M of salt was added, while in work³³ with the explicit media modeling the transition to A-DNA was registered in 1.5 nanoseconds with only 0.45M of salt added. Therefore we introduce ions explicitly.

Explicit modeling of solvent takes lion's share of computational resources, and we know of no evidence that interaction of DNA with solvent molecules should be treated explicitly. Therefore, all the known effects of the medium (electrostatics and solvation), which may affect the balance of interactions in the system, are represented implicitly, through effective potentials of interaction between the grains of the CG model, between the ions, and between the ions and the grains of the CG model.

1. Electrostatic interaction between phosphate grains: distance dependent permittivity $\varepsilon(r)$

The simplest way to model electrostatic forces between phosphates is to put negative charges ($-e$) on phosphate grains and to introduce the Coulomb potential of interaction between these charges. Because of the small distances between phosphates and because of the appreciable changes in the distances in B \leftrightarrow A transition one has to use a distance dependent permittivity $\varepsilon(r)$ in this potential. Indeed, the dielectric constant ε is close to vacuum at small distances between the charges because there are not enough solvent molecules between the phosphates for screening their charges. Therefore, ε is normally taken equal to 2-3 at small distances. With increasing distance r , $\varepsilon(r)$ is expected to reach its macroscopic value. Starting value and slope of this curve depend on size and dipole moment of solvent molecules, as well as on the

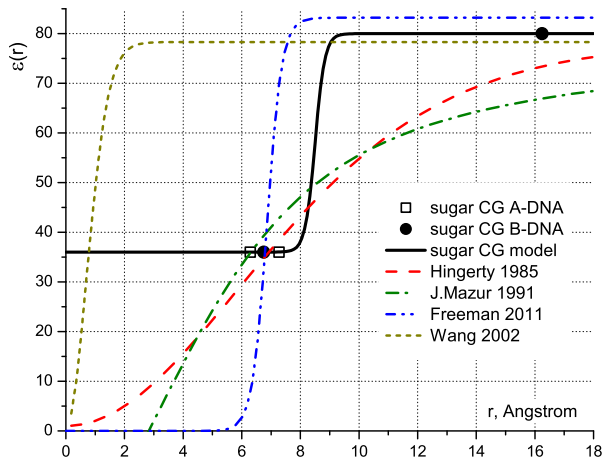


FIG. 6. Screening of phosphate charges: distance dependence of permittivity $\varepsilon(r)$ in the Coulomb potential of repulsion between negative charges on phosphate grains. We compare the dependence adopted in our model with the dependencies offered or used in other works: by Hingerty et al⁴³ for charges on biopolymers, by J. Mazur et al⁴¹ and by Wang et al⁴⁰ for all-atom B-DNA modeling, and by Freeman et al⁴² for a CG B-DNA. The points show the dielectric constants on MD trajectory of our sugar CG model for the nearest grains along the strand in A-DNA and B-DNA: $\varepsilon(6.29\text{\AA}) = 36$ and $\varepsilon(6.7\text{\AA}) = 36$, and for the nearest grains located across the major groove: $\varepsilon(7.3\text{\AA}) = 36$ (A-DNA), $\varepsilon(16.2\text{\AA}) = 80$ (B-DNA).

location of the charges on the DNA molecule.

One may use different analytical forms for the dependence $\varepsilon(r)$ (see a review in⁴⁰ and⁴¹). We adopted the simplest representation already used in one CG DNA model⁴²:

$$\varepsilon(r) = \varepsilon_0 + \varepsilon_1 \tanh\left[\exp\left(\frac{\alpha}{2}(r - r_0)\right)\right], \quad (2)$$

with differing parameters: $\varepsilon_0 = 58$ and $\varepsilon_1 = 22$, $\alpha = 12\text{\AA}^{-1}$, $r_0 = 8.5\text{\AA}$. This function is shown in fig. 6.

2. Interactions between ions, and between ions and DNA grains: solvation effects and sequence dependence

A-DNA can not be simulated in water with sodium counterions, even in a small box. The only exception we know of is in work³² where a B to A transition was observed in a tiny water drop in which the surface tension contributed to the formation of the compact A-DNA. Normally, one needs to add salt to DNA with counterions to observe an A-DNA (see, for example,³³). Therefore, in the CG model, we included explicit ions Na^+ and Cl^- and interactions between them, and between the ions and the charges on DNA.

We also found that the charges (-e) on phosphates are not sufficient for the formation of A-DNA, one needs to

TABLE II. Charges (in units of the elementary charge e) of base grains interacting with ions in solution.

type of base	B_1	B_2	B_3
Adenine	-0.048	0.109	-0.061
Thymine	0.390	-0.240	-0.150
Guanine	-0.496	0.134	0.362
Cytosine	0.433	0.061	-0.494

put partial charges on bases (on grains B_1 , B_2 , B_3 of all the bases), and so to introduce the sequence dependence. More exactly, the A-DNA conglomerate is not stable if there are no charges on bases keeping the sodium ions inside the major groove. Therefore, we distributed partial charges on grains so that the dipole moment of every (neutral) base coincided with the moment in the AMBER force field (table II).

One can obtain effective potential of interaction between ions in a solvent from a radial distribution function (rdf) in an all atom simulation by several different methods⁴⁴⁻⁴⁷. These methods yield the potentials of close shapes. We chose the analytical representation of the potential function proposed in⁴⁷:

$$\mathcal{V}_{ij} = \frac{A}{r_{ij}^{12}} + \sum_{k=1}^5 D_k \exp^{-C_k[r_{ij} - R_k]^2} + \frac{q_i q_j}{4\pi\epsilon_0 \varepsilon r_{ij}}, \quad (3)$$

where r_{ij} is the distance between i th and j th particles (between ions or between an ion and a DNA grain). In this expression, the first term introduces excluded volume, the second term describes the shape of peaks and minima of the potential due to solvation, and the last term is the long-distance asymptotics: electrostatic (Coulombic) interaction between the charges.

We adopted $\text{Cl}^- - \text{Na}^+$ and $\text{Cl}^- - \text{Cl}^-$ potentials obtained in work⁴⁵ from all atom simulation of 0.5M NaCl electrolyte. In the simulation the authors used the Smith-Dang's ion model⁴⁸. Because we have few Cl^- ions interacting mostly with Na^+ ions and one with another, we assumed that we may use these potentials, even with a DNA molecule added in solution. For the interactions of Cl^- ions with phosphate grains $\text{Cl}^- - \text{P}^-$, we adopted the potential obtained in⁴⁴, again from all atom simulations with the Smith-Dang's ion model. We also used $\text{Na}^+ - \text{Na}^+$, $\text{Na}^+ - \text{Cl}^-$ and $\text{Cl}^- - \text{Cl}^-$ potentials from⁴⁵ as templates for potentials of interaction between ions and grains on bases. The details of the derivation of these potentials are in Appendix B (section VIII).

Potentials of interaction between sodium ions and between sodium ions and phosphate grains were chosen so that there were both A-DNA and B-DNA, as well as both $\text{A} \rightarrow \text{B}$ and $\text{B} \rightarrow \text{A}$ transitions in the model. In figures 7 and 8 we compare these potentials with the ones obtained by different methods or exploited in some works.

Parameters $\{A, D_k, C_k, R_k\}$ of the potentials used in our CG model are listed in tables X-XV in Appendix B (section VIII). We showed some of the potential curves in figures 19 and 20.

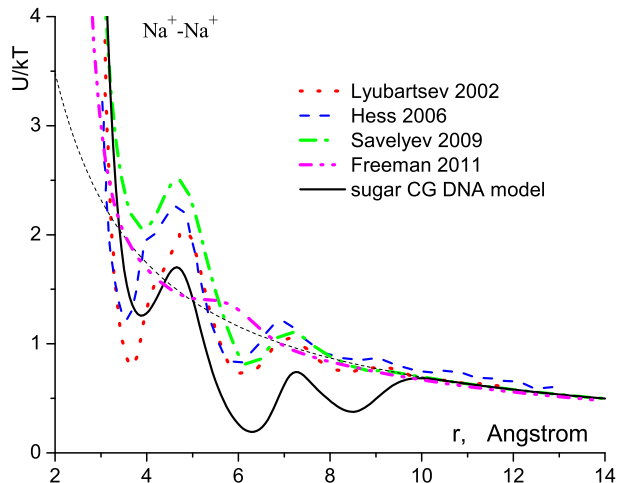


FIG. 7. Comparison of effective potentials of sodium ions interaction. The solid line corresponds to the potential used in the sugar CG DNA model. Dotted, dashed and dash-dotted lines represent the potentials obtained by different methods from all-atom simulations of ions in aqueous solution of salt in works by Lyubartsev et al⁴⁵, Hess et al⁴⁶, Savelyev et al⁴⁷. We also show the potential used in CG modeling of B-DNA by Freeman et al⁴² - dash-dot-dot line. Thin dashed curve corresponds to the Coulombic interaction between the charges (the last term in equation (3)).

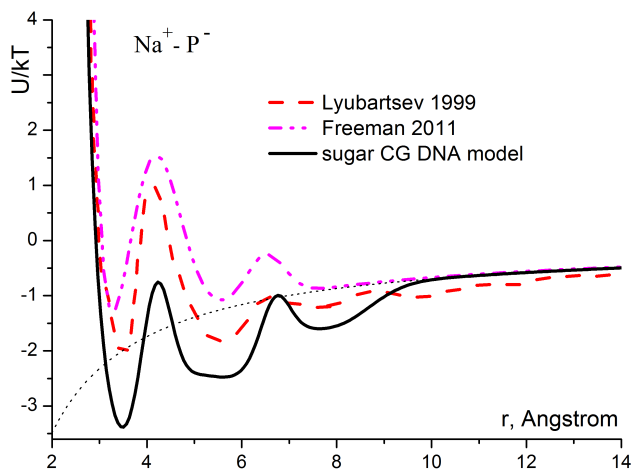


FIG. 8. Comparison of effective potentials of interaction between phosphate grain and sodium ion. The potential used in the sugar CG model - solid line, the one obtained by Lyubartsev et al⁴⁴ from all-atom simulation of B-DNA - dashed line; the one used in CG modeling of B-DNA by Freeman et al⁴² - dash-dot-dot line. Thin dashed curve corresponds to the Coulombic interaction between the charges (the last term in equation (3)).

3. Interaction of ions with grains C1', C3' and grains of bases: excluded volume

We did not put charges on the grains C1' and C3', and the ions interact with them only by excluded volume potential. We estimated the value of this volume from the rdf-s between sodium ions and atoms belonging to these grains. These functions had been obtained in papers^{44,49} for some atoms on bases and atoms O4' (belonging to the grain C1') and C4' (belonging to the grain C3') from all atom MD trajectories of B-DNA. For the atom O4', solvation peaks are very low, and the rdf approaches unity at 4.5Å (and this is true for all the uncharges grains). We neglect a very low peak between 2.3 and 3.5Å, and accept that the rise of the rdf begins at 3.5Å. We take this value as the distance of closest approach between a Na⁺ ion and the grain C1'. Similarly, for the grain C3', excluded volume distance is equal to 3.2Å.

Leaning upon these estimates, we accepted the following potential functions for the excluded volume interactions of sodium ions with the uncharged grains C1' and C3':

$$\begin{aligned} E_{Na^+-C1'} &= \epsilon (\sigma_{C1'}/r)^{16}, \\ E_{Na^+-C3'} &= \epsilon (\sigma_{C3'}/r)^{12}, \end{aligned} \quad (4)$$

with $\sigma_{Na^+-C1'}=3.5\text{\AA}$, $\sigma_{Na^+-C3'}=3.2\text{\AA}$ and the same $\epsilon=0.369\text{ kcal/mol}$ ($\approx 0.6\text{kT}$ at $T=25^\circ\text{C}$).

For the potentials for the excluded volume interactions of chlorine ions with the uncharged grains C1' and C3' we used the same functions, only with $\sigma_{Cl^- - C1'} = \sigma_{Cl^- - C3'} = 3.3\text{\AA}$.

4. Interaction of ions and grains of DNA with implicit water: coefficient of friction

Influence of water molecules on solute molecules within implicit solvent representation is normally simulated by Langevin equation. It provides both thermostat and viscosity. If one takes damping (friction) coefficient $\gamma=70\text{ ps}^{-1}$ for sodium ions in implicit water, their diffusion coefficient proves to be equal to the experimental value. In work⁵⁰, DNA atoms, fully exposed to water, had the same damping coefficient $\gamma=70\text{ ps}^{-1}$, while completely buried DNA atoms had a zero coefficient (no Langevin term). Partially exposed atoms had a damping coefficient proportional to the fraction of its solvent exposed surface area. In work³⁹, γ was equal to 50 ps^{-1} for all DNA atoms, while in work⁵¹ - to 5 ps^{-1} .

The value of the damping coefficient influences the rate of relaxation processes which depend on the solvent. This value does not seem to affect the balance of interactions in DNA molecule. We made simulations with small friction $\gamma=5\text{ ps}^{-1}$ for both DNA grains and ions to make rapid system relaxation or to follow the behavior of the system for effectively longer time periods. To observe the behavior comparable with the all atom simulation on

its timescale, we used big friction $\gamma_1 = 50\text{ps}^{-1}$ for DNA grains and $\gamma_2 = 70\text{ps}^{-1}$ for ions.

III. DESCRIPTION OF THE SUGAR CG DNA MODEL

In the sugar CG DNA model (see fig.5), every one of the two DNA strands is modeled by a zigzag of alternating grains P and C3': ...-P-C3'-P-C3'-... These grains are connected by "valence" bonds. A grain C1' is linked to each C3' grain by another "valence" bond. This "comb" is a skeleton of the strand. The grain C1' and the grains on the base B1, B2, B3 are connected by very rigid "valence" bonds C1'-B1, C1'-B3, B1-B2, B2-B3, B2-B3. We keep grains C1', B1, B2 and B3 in one plane by means of rigid "torsion" angle C1'-B1-B3-B2. The three rigidly bound grains (B1, B2, B3) almost freely rotate around glycosidic bond C1'-N(1,9) (position of the atom N(1,9) is calculated on each step from coordinates of the grains B1, B2, B3).

To maintain the shape of the helix ...-P-C3'-P-C3'-..., we introduce, besides the "valence" bonds, the "valence" angle C3'-P-C3' and two "torsion" angles C3'-P(2)-C3'-P(3) and P(1)-C3'-P(2)-C3'. The position of the glycosidic bond C1'-N(1,9) relative to the "skeleton" helix is supported by two "valence" angles P(1)-C1'-N(1,9) and C3'-C1'-N(1,9). Another "torsion" angle C1'-C3'-P(2)-C3' provides base pair opening.

Ribose flexibility is modeled by deformation of the pyramid {P(1)P(2)C1'C3'}. The possibility of the sugar repuckering is provided by a double-well potential for the "valence" bond C1'-P(2). The length of the edge P(1)-P(2) correlates with length of the "double-well" bond. The grains P(1) and C1' are connected by a soft "valence" bond.

The model system consists of a DNA double helix and explicit sodium and chlorine ions. The potential energy of the system includes ten contributions:

$$\begin{aligned}
 H = & E_{base} + E_{hydr-bonds} + E_{stacking} + \\
 & + E_{val-bonds} + E_{val-angles} + E_{tors-angles} + \\
 & + E_{el} + E_{vdW} + E_{ion-DNA} + E_{ion-ion} \quad (5)
 \end{aligned}$$

The corresponding potential functions and the used parameters are collected in table III.

The term E_{base} describes the energy of deformation of rigid bases. The terms $E_{hydr-bonds}$ and $E_{stacking}$ stand for energy of hydrogen bonds between complementary bases and for base pairs stacking, correspondingly. We recalculate the coordinates of all nucleobase atoms on each step and compute these terms using the all atom force field AMBER.

The terms $E_{val-bonds}$, $E_{val-angles}$, $E_{tors-angles}$ describe energy of deformation of "valence" bonds, "valence" angles and "torsion" angles on the strands of CG DNA. Equilibrium values of the angles and the bonds, not pertaining to the ribose flexibility, were chosen equal to the values in A-DNA. For the rigidities were chosen the

maximal values. Two wells in the double-well potential of the bond C1'-P(2) were made of equal depth, contrary to the AMBER force field (see fig. 18). We discuss the reason for these choices in section V.

Coulombic interactions E_{el} between charged phosphate grains have distance dependent permittivity (see formula (2)). We introduce van der Waals interactions E_{vdW} for the grains P and C3' not connected through "valence" bonds, "valence" angles or "torsion" angles.

Interaction of ions with DNA $E_{ion-DNA}$ includes interactions with charged phosphate grains P and grains on bases and with uncharged grains (C1', C3'). In the present realization of the model, we introduce sequence dependence: the charges on grains of a base depend on the type of this base. Interactions of ions one with another $E_{ion-ion}$ and with charges on DNA (phosphate grains and grains on bases) $E_{ion-DNA}$ take into account solvation effects (besides direct Coulomb force).

The influence of water on DNA and on ions is described implicitly, by Langevin equation. Damping constant (friction) is taken to be equal to 5ps^{-1} for system relaxation and test calculations. Productive runs were made with $\gamma=5\text{ps}^{-1}$, as well as with $\gamma_1=50\text{ps}^{-1}$ for the DNA grains and $\gamma_2=70\text{ps}^{-1}$ for the ions.

IV. MODEL TESTING

We found two equilibrium states (A-DNA and B-DNA) of the system by its energy minimization (from different initial states at corresponding boundary and initial conditions). After this, we compared CG MD trajectories with the ones obtained in all atom simulations.

A. Energy minimization: A-DNA and B-DNA.

To obtain the ground states of B- and A-DNA, we started from all atom MD configurations of DNA in water and in mixed ethanol/water (85/15) solution correspondingly. We put the grains and ions of our CG model on the places of the corresponding atoms and ions of the all atom system. We also added 16 Na^+ and 16 Cl^- ions for A-DNA. For more adequate comparison with A-DNA, we studied B-DNA not only in combination with counterions (which is common), but also with the same amount of additional salt as for A-DNA. The additional ions were placed randomly in the unoccupied area of the computational cell. We modeled B-DNA in a large reservoir: a cube $60 \times 60 \times 60 \text{\AA}$. In this volume, the 32 salt ions give the molar concentration 0.12M, very close to the one of physiological saline. For A-DNA, we chose a small volume so that, on the one hand, the ions could not go too far from the molecule, and, on the other hand, the energy of interaction between the chlorine ions and the phosphate grains was not too high. The optimal reservoir proved to be a cylinder with diameter 18.5\AA and height 30\AA . In it, the salt concentration was 0.8M. The energy of the

TABLE III. A summary of the potential functions and parameters of the sugar CG DNA model. The order of grains in the notation of bonds and angles is their order along the chain direction (see fig. 5). The letter N stands for atom $N1$ (or $N9$), and C - for atom $C6$ (or $C8$) on bases.

Interaction	Potential	Constants	
"valence" bonds		$r_0, \text{\AA}$	$k_r, \text{kcal}/(\text{mol} \cdot \text{\AA}^2)$
P-C3'		4.52	35
C3'-C1'	$\frac{1}{2}k_r(r - r_0)^2$	2.4	192
C3'-P		2.645	201
P-C1'		5.4	28
double-well "valence" bond (imitating ribose flexibility)			
	parameter	value	dimension
	r_A	4.8	\AA
	r_B	4.2	\AA
	r_C	4.584	\AA
C1'-P	$U(r) = U_B(r - r_B)f(r) + [U_A(r - r_A) + \epsilon_0][1 - f(r)] + \epsilon_{\text{barrier}}e^{-\mu_0(r-r_C)^2}$	ϵ_0	kcal/mol
	$U_j(r) = \frac{1}{2}K_jr^2, j = A, B$	$\epsilon_{\text{barrier}}$	kcal/mol
	$f(r) = \frac{1}{1+e^{2\mu(r-r_C)}}$	K_A	kcal/(mol $\cdot \text{\AA}^2$)
		K_B	kcal/(mol $\cdot \text{\AA}^2$)
		μ	\AA^{-1}
		μ_0	\AA^{-1}
"valence" bond correlated with ribose conformation			
	parameter	value	dimension
P(1)-P(2)	$U(r_{C1'P}, r_{P(1)P(2)}) = \frac{1}{2}k_P(r_{P(1)P(2)} + t_P r_{C1'P} - l_{P0})^2$	k_P	kcal/mol
		l_{P0}	\AA
		t_P	
"valence" angles			
		θ_0, deg	$k_\theta, \text{kcal}/(\text{mol} \cdot \text{deg}^2)$
C3'-P-C3'		110	0.017
P-C1'-N	$\frac{1}{2}k_\theta(\theta - \theta_0)^2$	84	0.026
C3'-C1'-N		112	0.032
"torsion" angles			
		δ_0, deg	$\epsilon_\delta, \text{kcal}/\text{mol}$
C3'-P-C3'-P		188	4.6
P-C3'-P-C3'	$\epsilon_\delta(1 - \cos(\delta - \delta_0))$	194	4.6
C1'-C3'-P-C3'		13	3.0
C3'-C1'-N-C		-32	0.03
interactions in rigid bases			
bonds	$\frac{1}{2}k_r(r - r_0)^2$		see formula (B4)
torsion angle	$\epsilon(1 + \cos \delta)$		and table III in ²²
hydrogen bonds and stacking interactions			
		from AMBER	
electrostatic interactions between phosphate grains			
	parameter	value	dimension
$P - P$	$\frac{q_i q_j}{4\pi\epsilon_0\epsilon(r)r_{ij}}$	ϵ_0	22
	$\epsilon(r) = \epsilon_0 + \epsilon_1 \tanh[\exp(\frac{\alpha}{2}(r - r_0))]$	ϵ_1	58
		α	0.3
		r_0	\AA
van der Waals interactions between skeleton grains			
	parameter	value	$\epsilon_i, \text{kcal}/\text{mol}$
P	$4\epsilon_{ij} \left[\left(\frac{\sigma_{ij}}{r}\right)^{12} - \left(\frac{\sigma_{ij}}{r}\right)^6 \right]$	2.18	0.23
$C3'$	$\sigma_{ij} = (\sigma_i + \sigma_j)/2, \epsilon_{ij} = \sqrt{\epsilon_i \epsilon_j}$	2.0	0.115
interaction of Na^+ and Cl^- ions with charged grains of DNA and one with another			
		$q_{\text{Na}^+} = +e, q_{\text{Cl}^-} = -e, q_P = -e,$	
		charges of grains of bases see in table II;	
		A, D_k, C_k, R_k, ϵ are in tables X, XI, XII, XIII, XIV, XV	
interaction of ions with uncharged grains			
	parameter	value	$\epsilon, \text{kcal}/\text{mol}$
Na^+ with C1'	$\epsilon(\sigma/r)^{16}$	3.5	0.369
Na^+ with C3'	$\epsilon(\sigma/r)^{12}$	3.2	0.369
Cl^- with C1'	$\epsilon(\sigma/r)^{16}$	3.3	0.369
Cl^- with C3'	$\epsilon(\sigma/r)^{12}$	3.3	0.369

CG system was minimized by the method of conjugate gradients: first the ions, and then the whole system. As a result, we obtained both CG A- and B-DNA conformations (in proper computational cells) which we used as initial configurations for MD simulations.

B. MD simulations of sugar CG A-DNA and B-DNA.

For MD simulations, we exploited the Runge-Kutta method, with a Langevin thermostat. As a boundary condition, we used the condition of reflection of ions from the sides of the computational cell. The initial configurations of the system were the ones obtained by energy minimization described in section IV A.

The initial system relaxation was being done in two stages. First, during one nanosecond, we carried out a relaxation of the ion atmosphere with the DNA molecule kept immobile. Then, the whole system was relaxing during the next 0.5 nanoseconds. During all the relaxation process, the friction for all the grains and ions was $\gamma = 5\text{ps}^{-1}$. The productive runs were carried out both with the small friction $\gamma = 5\text{ps}^{-1}$, and with the large friction $\gamma_1 = 50\text{ps}^{-1}$ for the DNA grains and $\gamma_2 = 70\text{ps}^{-1}$ for the ions.

We followed the dynamics of the both forms, A- and B-DNA, at temperature 300 K up to 8 nanoseconds with small friction and up to 18 nanoseconds with large friction, which allows to consider the forms stable at the corresponding conditions. B-DNA is stable in both the simulations: with counterions and in physiological saline. The obtained stable configurations are shown in figure 9. The balance of interactions in A-DNA and B-DNA is presented in histogram in fig. 10.

Tables IV and V present the lengths and the angles in the sugar CG model in comparison with the all atom AMBER model. As one should expect, our model proved to be stiffer than the all atom one (we accepted the maximal rigidities observed in all atom simulations), and the angles in both A- and B-DNA are closer to their values in all-atom A-DNA (so we set them). The only exception is torsion $\angle C3'C1'NC$, for which the prescribed magnitude was (-32°) , while the observed one (-50°) in A-DNA and (-40°) in B-DNA. Interestingly, that the value for A-DNA is in excellent agreement with the crystallographic value (GLACTONE³⁰): see table IX.

Figures 11 and 12 give a visualization of the ribose flexibility in CG A- and B-DNA. One can see that the CG model imitates the AMBER A-DNA very closely, including sequence dependence. Sugar CG B-DNA is stiffer and has lower population in the area between C2'-endo and C3'-endo.

A-DNA can exist only if sodium ions can assemble in the major groove so that their electrostatic interaction with the phosphate grains (and with the nearest chlorine ions) will give the gain in free energy greater than the loss in entropic contribution because of the ion clustering (see the balance of interactions in CG DNA forms in

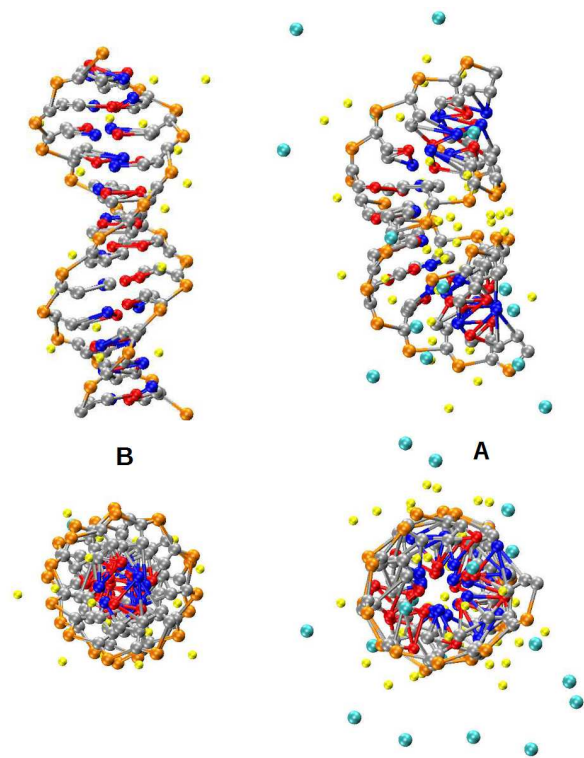


FIG. 9. Frames from the trajectories of sugar CG A-DNA (on the right) and B-DNA (on the left). Temperature is 300 K. Sodium ions are yellow, chlorine - cyan.

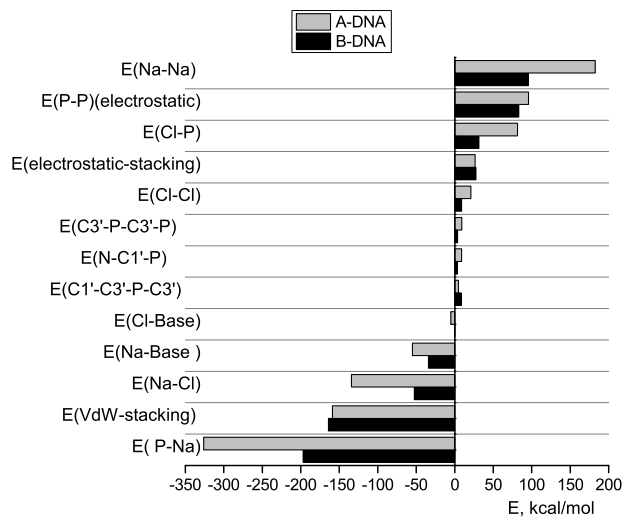


FIG. 10. Comparison of the average contributions to the full potential energy of the CG A-DNA and B-DNA. Both the systems consist of a DNA molecule, counterions and additional salt (16 sodium and 16 chlorine ions). The temperature is 300 K. B-DNA is in a cube $60 \times 60 \times 60 \text{\AA}$, A-DNA is in a cylinder with diameter 18.5\AA and height 30\AA .

TABLE IV. Comparison of lengths and angles in the sugar CG A-DNA (with small friction $\gamma=5\text{ps}^{-1}$) in concentrated salt solution and in the all atom AMBER A-DNA in mixed ethanol/water (85/15) solution. The letter N stands for atom $N1$ (or $N9$), and C - for atom $C6$ (or $C8$) on bases. The averages were taken over a trajectory of 8 nanoseconds long for the CG model, and of 4.5 nanoseconds long for the all atom model.

value	dimension	sugar-CG model	AMBER
$ PC3' $		4.5 ± 0.1	4.5
$ C3'C1' $		2.40 ± 0.05	2.4
$ C3'P $	Å	2.65 ± 0.05	2.6
$ PC1' $		5.4 ± 0.1	5.4 ± 0.3
$ C1'P $		4.7 ± 0.1	4.8 ± 0.2
$ P(1)P(2) $		6.3 ± 0.2	6.1 ± 0.8
$\angle C3'PC3'$		109 ± 4	110 ± 14
$\angle PC1'N$	deg	83 ± 3	84 ± 10
$\angle C3'C1'N$		112 ± 3	112 ± 3
$\angle C3'PC3'P$		173 ± 14	173 ± 32
$\angle PC3'PC3'$	deg	213 ± 11	217 ± 30
$\angle C3'C1'NC$		-50 ± 11	-32 ± 9

TABLE V. Comparison of lengths and angles in the sugar CG B-DNA (with small friction $\gamma=5\text{ps}^{-1}$) and in the all atom AMBER B-DNA. The letter N stands for atom $N1$ (or $N9$), and C - for atom $C6$ (or $C8$) on bases. The averages were taken over a trajectory of 8 nanoseconds long for the CG model, and of 20 nanoseconds long for the all atom model.

value	dimension	sugar-CG model	AMBER
$ PC3' $		4.5 ± 0.1	4.53
$ C3'C1' $		2.40 ± 0.05	2.368
$ C3'P $	Å	2.65 ± 0.05	2.66
$ PC1' $		5.4 ± 0.1	5.35 ± 0.4
$ C1'P $		4.3 ± 0.1	4.4 ± 0.4
$ P(1)P(2) $		6.8 ± 0.2	6.8 ± 0.6
$\angle C3'PC3'$		110 ± 4	104 ± 13
$\angle PC1'N$	deg	83 ± 3	105 ± 14
$\angle C3'C1'N$		113 ± 3	146 ± 13
$\angle C3'PC3'P$		186 ± 16	170 ± 31
$\angle PC3'PC3'$	deg	198 ± 12	211 ± 44
$\angle C3'C1'NC$		-40 ± 10	-27 ± 34

fig. 10). For the stabilization of this positively charged cluster between two rows of negative charges, the presence of a solvent in the major groove is crucial.

To adequately model this balance, one should very precisely choose the positions and the widths of the minima of the effective solvent-mediated potentials. We built our potentials for the $\text{Na}^+\text{-P}^-$ and $\text{Na}^+\text{-Na}^+$ pairs so that the CG radial distribution functions $g(r)$ were as close as possible to the all atom (AMBER) ones, especially in what regards the positions of the minima. The agreement between the CG rdf and the all atom one for the pair $\text{Na}^+\text{-P}^-$ is almost ideal (see fig.13). For the pair $\text{Na}^+\text{-Na}^+$ it was impossible because we simulated A-DNA in water, and not in mixed ethanol/water solution. A-DNA with counterions in water does not exist without additional salt. Therefore we had many more sodium ions in the computational cell, and, correspondingly, in the ma-

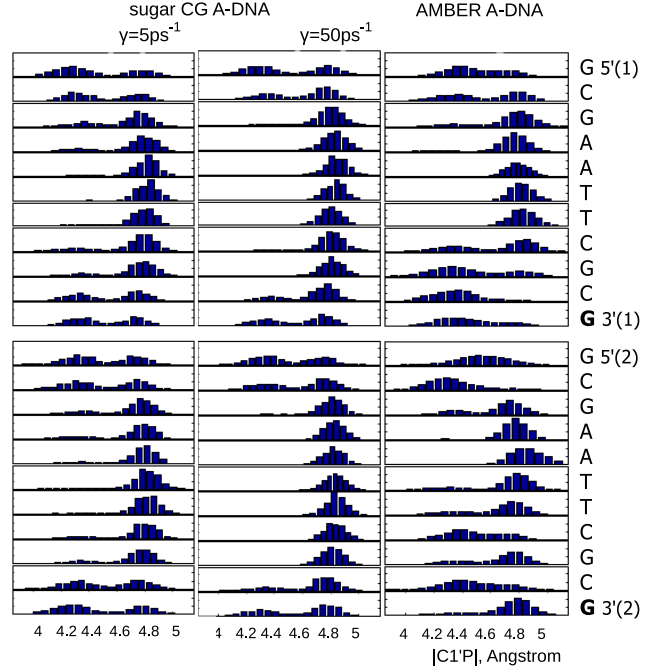


FIG. 11. Ribose flexibility of A-DNA in the sugar CG model with both small ($\gamma=5\text{ps}^{-1}$) and large ($\gamma=50\text{ps}^{-1}$) friction in concentrated salt solution *vs.* ribose flexibility of A-DNA in the all atom AMBER model in mixed ethanol/water (85/15) solution. We show histograms of the length of the bond $C1'P$ which directly correlates with the pseudorotation angle. The histograms were plotted for the counts at every 1ps over the trajectories 4.5 nanoseconds long.

ior groove. It had to lead to the substantial rise of the first peak as compared with the second one (see fig.14), which usually takes place with increase of the salt concentration (see, for example,⁵²). However, our $\text{Na}^+\text{-P}^-$ and $\text{Na}^+\text{-Na}^+$ pairs are more sticky than the default AMBER ions. One can see that from rdFs for B-DNA shown in fig. 15 and 16.

Because of the problems of choice of ion parameters in the framework of additive, nonpolarizable and pairwise potentials, there are several different sets of ion parameters. Aqvist's cations and Dang's Cl^- , which were used in AMBER by default, give the artefact of formation of stable ion pairs and even salt crystals at moderately low concentrations (below their solubility limit). Other sets of the parameters result in rdFs greatly differing in shape (see fig. 6 in⁵³).

As compared with default AMBER ions, our CG model gives for the pair $\text{Na}^+\text{-P}^-$ a very high first peak (see fig. 15), which means that our Na^+ ions are more often located near phosphates, and, consequently, one to another (see fig. 16). Rdf for the $\text{Na}^+\text{-P}^-$ pair for B-DNA in our model mostly resembles the corresponding rdf for Cheatham's ions⁵⁴. When compared to the others, Cheatham's sodium ions are much more often near

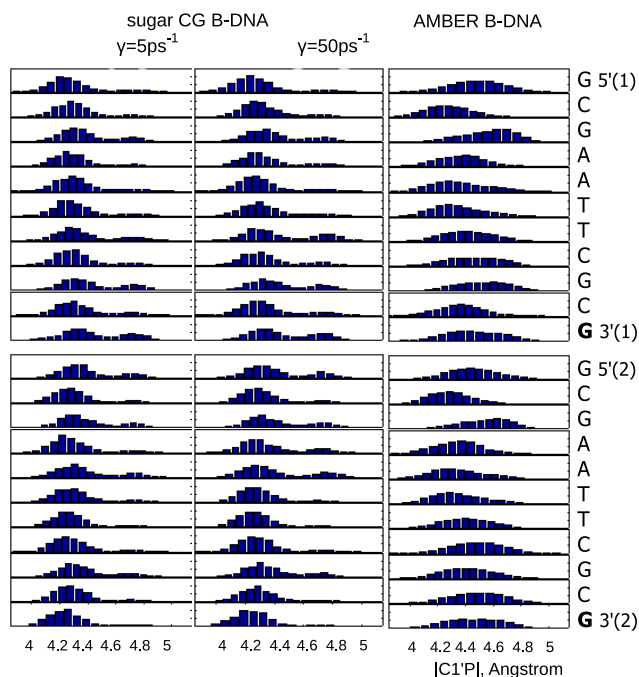


FIG. 12. Ribose flexibility of B-DNA with counterions in the sugar CG model with both small ($\gamma=5\text{ps}^{-1}$) and large ($\gamma_1=50\text{ps}^{-1}$) friction *vs.* ribose flexibility of B-DNA in the all-atom AMBER model. We show histograms of the length of the bond C1'P which directly correlates with the pseudorotation angle. The histograms were plotted for the counts at every 1ps over the trajectories 20 nanoseconds long.

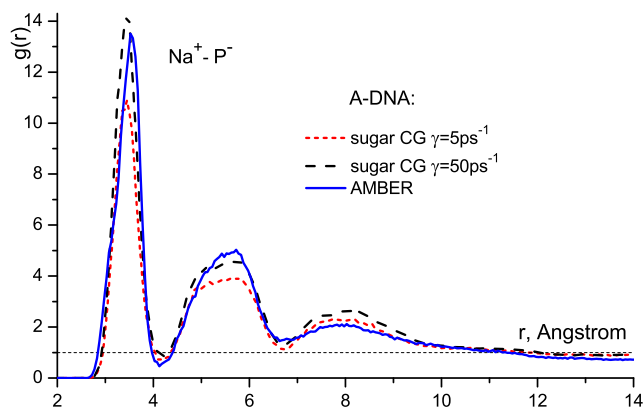


FIG. 13. Radial distribution function $g(r)$ of Na^+ ions around phosphate grains P^- in the sugar CG A-DNA with both small (short dashed line) and large (dashed line) friction of grains γ . For comparison, we show $\text{Na}^+ - \text{P}^-$ distribution function in the all-atom AMBER model of A-DNA in mixed ethanol/water solution (solid line).

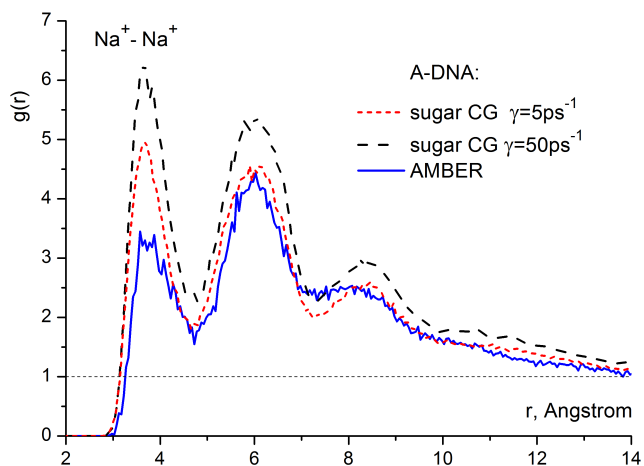


FIG. 14. Radial distribution function $g(r)$ of the pair $\text{Na}^+ - \text{Na}^+$ in the sugar CG A-DNA with both small (short dashed line) and large (dashed line) friction of grains γ . For comparison, we show this distribution function in the all-atom AMBER model of A-DNA in mixed ethanol/water solution (solid line).

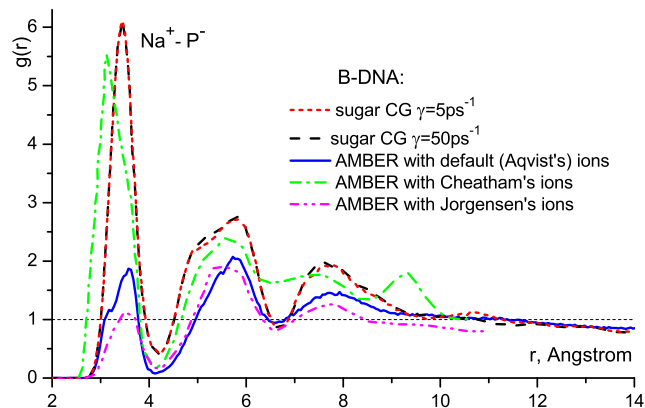


FIG. 15. Radial distribution function $g(r)$ of Na^+ ions around phosphate grains P^- in the sugar CG B-DNA (without additional salt) with both small (short dashed line) and large (dashed line) friction of grains γ . For comparison, we show $\text{Na}^+ - \text{P}^-$ distribution functions in the all-atom AMBER model of B-DNA with different parameters for ions: default Aqvist's (solid line), Cheatham's (dash-dot line)⁵³ and Jorgensen's (dash-dot-dot line)⁵³.

phosphates, avoiding chlorine ions and each other (see fig. 11 and 6 in⁵³). This feature seems to be a drawback leading to over-neutralization of the DNA. However, it proved⁵⁵ to be that the number of Cheatham's sodium ions well agrees with ion counting experiments at low salt concentrations, and at high concentrations ($>0.7\text{M}$) is even less than in experiment. Therefore, we can regard our effective potentials for ion interactions as trustworthy.

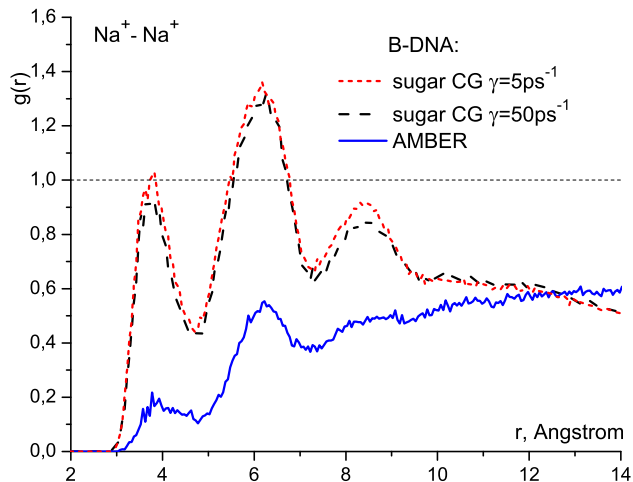


FIG. 16. Radial distribution function $g(r)$ of the pair Na^+-Na^+ in the sugar CG B-DNA (without additional salt) with both small (short dashed line) and large (dashed line) friction of grains γ . For comparison, we show this distribution function in the all-atom AMBER model of B-DNA (solid line).

V. DISCUSSION AND CONCLUSION

We built our CG model on the base of the all atom force field AMBER, and we still keep the all-atom base pairing and stacking (it should be changed to a CG version). Starting from AMBER, we faced the problem that our CG DNA can assume a B-form structure at almost every reasonable set of parameters, while balancing interactions in the A-DNA required some efforts.

First, we supposed that an A-DNA can exist without placing partial charges on the bases, i.e. without introduction of sequence dependence. But that proved to be impossible. At temperature only as high as 300 K, the conglomerate of A-DNA proved to be unstable, the charges on the borders of the major groove were insufficient to keep the ions inside this groove.

Secondly, the potentials and the constants, derived from the AMBER force field, required corrections. Namely, for all the bonds and the angles (except for C1'P and P(1)P(2) connected with ribose flexibility) we used equilibrium values of the all-atom A-DNA and maximal rigidities observed in the all-atom simulations. For the double-well potential of the bond C1'P we lower the A-minimum to the level of the B-minimum (see fig. 18). In this connection, one can remember work³⁷, where, to provide in AMBER force field a spontaneous B to A transition of $d[\text{CCAACGTTGG}]_2$ sequence in 85% ethanol solution, the authors had to make "reduction of the V2 term in the O-C-C-O torsions from 1.0 to 0.30 kcal/mol to better stabilize the C3'-endo sugar pucker".

Finally, we had to exploit such effective potentials between sodium ions and phosphate grains and between sodium ions one with another that resulted in a rdf for

the pair Na^+-P^- very close to the rdf for Cheatham's ions (see fig. 15), and not for default AMBER ions (for more details, see the discussion at the end of section IV B).

Evidently, the necessity of these corrections is a result of the long known B-philia of the AMBER force field (see, for example,⁵⁶). Indeed, the B \rightarrow A transition at high salt concentration has been demonstrated for the A-philic CHARMM force field in 1996, while for the AMBER force field this transition in water takes place only in a tiny drop of water³². In it, the compact A-DNA is stabilized by surface tension. The additional salt results only in salt crystallization, instead of causing the transition.

After the described fitting, we have obtained both an A-DNA and a B-DNA at the corresponding conditions, as well as both A \rightarrow B and B \rightarrow A transitions. The chosen set of parameters, providing the needed balance, is, of course, not unique and, may be, not yet quite adequate. It will probably be corrected in the process of application of the CG model to different physical situations.

The offered sugar CG model is adequate, physically clear, computationally cheap, allows to promptly check physical hypotheses, and so can be employed for the study of many interesting problems, including the cases in which all atom DNA models can not be used. For example, the CG model can be applied for investigation of large mechanical deformations of long DNA molecules (when they package into chromosomes). The introduced sequence dependence allows to use the model for studying of DNA-protein interactions, including the interactions with CG proteins. A small change of the potentials enables base opening, and offers the possibility to simulate DNA melting, and investigate transcription and replication. Another large area of applications - modeling of electrostatic interactions of DNA with different types of ions in different kinds of solutions.

VI. ACKNOWLEDGEMENTS

We are sincerely grateful to our colleagues, prof. Alexey Onufriev (Virginia, USA) who obtained a trajectory of B-DNA in water for us; prof. Modesto Orozco (Barcelona) and Agnes Noy who kindly granted us a trajectory of A-DNA obtained in work⁵⁷; and U. Deva Priyakumar who sent us .pdb-files of DNA molecule with an opening base from work⁵⁸. For the realization of the sugar CG DNA model we used the (properly modified) program written by Dr. A.V. Savin. We take the opportunity to thank A.V. Savin for his help in the modification of the program. The simulations were partly carried out in the Joint Supercomputer Center of Russian Academy of Sciences. We appreciate financial support of RFBR (grants 12-03-31810 mol-a and 08-04-91118-a) and CRDF (award RUB2-2920-MO-07).

VII. APPENDIX A: DETAILS OF OBTAINING SUGAR CG DNA MODEL PARAMETERS FROM ALL-ATOM MD SIMULATIONS (AMBER)

"Relaxation" method shows that, under deformation of the bond P(1)-C3', the torsion angles change first: β , then α and γ , and one can observe *trans-gauche* transitions in these angles, and several different minima of the potential. If we neglect the α/γ -mobility, the potentials for this bond may be approximated by a parabola. In MD simulations, the lengths $|C3'C1'|$, $|C3'P(2)|$ and $|P(1)C3'|$ (see fig. 5) only slightly fluctuate for all the nucleotides. The estimates of the lengths and the rigidities made by different methods (see section IID) are listed in table VI.

For B-DNA in water, there are few nucleotides for which pseudorotation angle τ is localized in classical south region. For most nucleotides τ changes considerably, and in the process the pucker often is in the north region (characteristic for A-DNA) or, even more commonly, in the intermediate area. In contrast, the angle τ for A-DNA in the mixture of ethanol and water is well localized in the canonical north region. One can observe jumps to the south region, but the pucker is practically never in the intermediate area. On the other hand, the correlation between the distance $|C1'P(2)|$ and the pseudorotation angle is approximately the same. For the convenience of the analysis of correlations between the pseudorotational angle and the lengths $|P(1)C1'|$, $|C1'P(2)|$ and $|P(1)P(2)|$ we used the MD trajectory of A-DNA where two main ribose conformations are divided more distinctly. Figure 17 shows the behaviour of the bonds in pyramid $\{P(1)P(2)C3'C1'\}$ containing the sugar ring. As we expected (see IIC), only the length $|C1'P(2)|$ unambiguously correlates with τ , therefore we assigned a double-well potential to it.

TABLE VI. Lengths of "valence" bonds not connected with sugar repuckering (see fig. 5) and corresponding rigidities. We list (1) distances between the corresponding atoms in crystallographic (GLACTONE³⁰) A-DNA and B-DNA forms (l_{A-GI} and l_{B-GI}); (2) mean distances and rigidities l_{A-MD} , K_{A-MD} and l_{B-MD} , K_{B-MD} , obtained by Boltzmann inversion method from MD trajectories; (3) equilibrium lengths l_{relax} and rigidities K_{relax} of potentials obtained by method of "relaxation" (see IID). The distances have dimension of Angstroms, the rigidities - of kcal/(mol·Å²).

	$ C3'C1' $	$ C3'P(2) $	$ P(1)C3' $
l_{A-GI}	2.361	2.605	4.162
l_{A-MD}	2.40	2.645	4.52
K_{A-MD}	192	201	35
l_{B-GI}	2.368	2.609	4.072
l_{B-MD}	-	2.66	4.53
K_{B-MD}	-	222	19
$l_{A-relax}$	-	2.65	-
$K_{A-relax}$	-	230	-
$l_{B-relax}$	-	2.76	4.6
$K_{B-relax}$	-	288	16

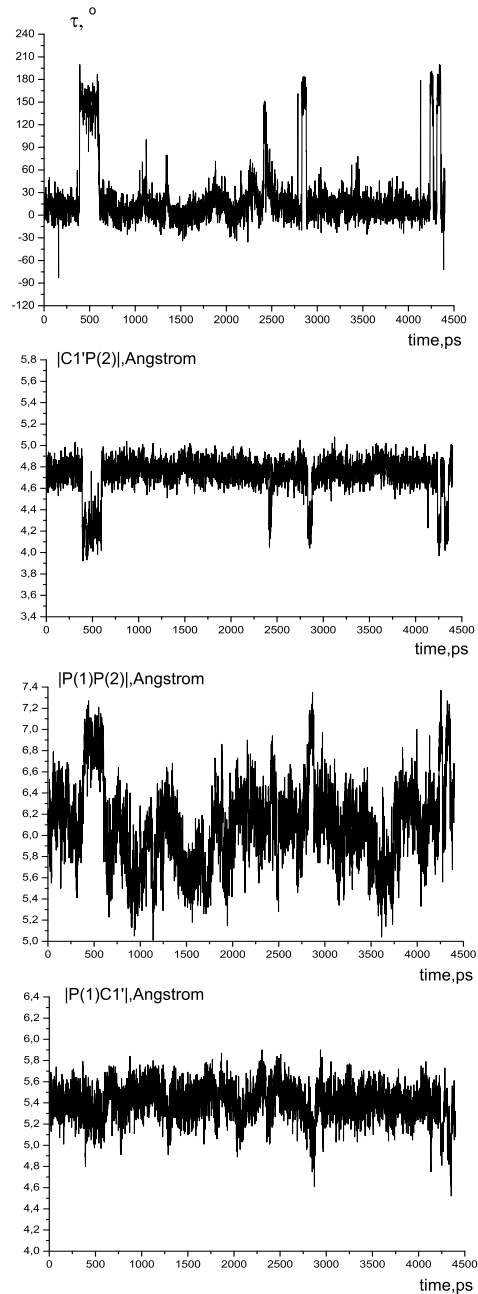


FIG. 17. Time dependence of the distances $|C1'P(2)|$, $|P(1)P(2)|$ and $|P(1)C1'|$ (see fig. 5) in comparison with the pseudorotational angle τ for the 4th nucleotide of the Dickerson-Drew dodecamer in A form in the mixture of ethanol and water (85:15) (parm99). Only the length $|C1'P(2)|$ correlates with the pseudorotation angle τ sufficiently strongly.

In table VII we list the mean lengths and the corresponding rigidities for the distances $|P(1)C1'|$, $|C1'P(2)|$ and $|P(1)P(2)|$, obtained from MD trajectories of A- and B-DNA forms.

We calculated the double-well potential of the bond C1'-P(2) by the method of "relaxation" (see the begin-

TABLE VII. Distances $|P(1)C1'|$, $|C1'P(2)|$ and $|P(1)P(2)|$ (see fig. 5) connected with sugar repuckering. We list characteristic and uncharacteristic values for these bonds and their rigidities obtained by Boltzmann inversion method from MD trajectories of A-DNA and B-DNA. In parentheses, we give the part of population (in per cent) near the characteristic and uncharacteristic values. In the cases when the division of the histogram into two peaks was difficult (the distances $|C1'P(2)|$ and $|P(1)P(2)|$ in B-DNA demonstrate one broad often non-symmetrical peak), we list simple means over nucleotides.

l_{A-Gl}		A	
$ P(1)C1' $,			
$l, \text{\AA}$	5.42	5.4 ± 0.34 (85%) //	5.0 ± 0.3 (15%)
$K_l, \frac{\text{kcal}}{\text{mol} \cdot \text{\AA}^2}$		19 ± 9 // 28 ± 6	
$ C1'P(2) $,			
$l, \text{\AA}$	4.59	4.8 ± 0.2 (64%) //	4.3 ± 0.3 (36%)
$K_l, \frac{\text{kcal}}{\text{mol} \cdot \text{\AA}^2}$		55 ± 17 // 27.4 ± 8	
$ P(1)P(2) $,			
$l, \text{\AA}$	5.63	6.14 ± 0.8 (75%) //	6.9 ± 0.4 (25%)
$K_l, \frac{\text{kcal}}{\text{mol} \cdot \text{\AA}^2}$		3.8 ± 1 // 18.4 ± 8	
l_{B-Gl}		B	
$ P(1)C1' $,			
$l, \text{\AA}$	4.89	5.35 ± 0.4 (84%) //	5.0 ± 0.35 (16%)
$K_l, \frac{\text{kcal}}{\text{mol} \cdot \text{\AA}^2}$		15 ± 5 // 19.5 ± 5	
$ C1'P(2) $,			
$l, \text{\AA}$	3.67	4.4 ± 0.4	
$K_l, \frac{\text{kcal}}{\text{mol} \cdot \text{\AA}^2}$		15 ± 3	
$ P(1)P(2) $,			
$l, \text{\AA}$	6.54	6.8 ± 0.6	
$K_l, \frac{\text{kcal}}{\text{mol} \cdot \text{\AA}^2}$		7 ± 2	

ning of section IID). We used a fragment of a DNA strand between two atoms C5' (including both of them and their hydrogen atoms); from the base we kept only one nitrogen atom, the nearest to the backbone. The obtained potential for $|C1'P(2)|$ is shown in fig. 18. The discontinuity of the function at distance around 5\AA is because the torsion angles of the fragment pass into the region inaccessible for DNA double helix. The two minima of the potential are 4.184\AA and 4.75\AA , the difference of energies in the minima - 0.7 kcal/mol , the barrier height - 1.9 kcal/mol , rigidities in the wells - 25 and 61 kcal/mol correspondingly. Comparing with the table VII, we see that the analysis of the MD trajectory for A-DNA gives very good estimates for lengths and rigidities in both wells, while in B-DNA the position of the left minimum is overestimated, and rigidity - underestimated (exactly as one would expect).

From table VIII one can see that the "valence" and "torsion" angles on the backbone (...-C3'-P-C3'-P-...) do not depend on sugar puckers.

The "valence" angles responsible for direction of the glycosidic bond relative to the backbone, as well as "torsion" angles for base pair opening and for rotation of base around the glycosidic bond are presented in table IX.

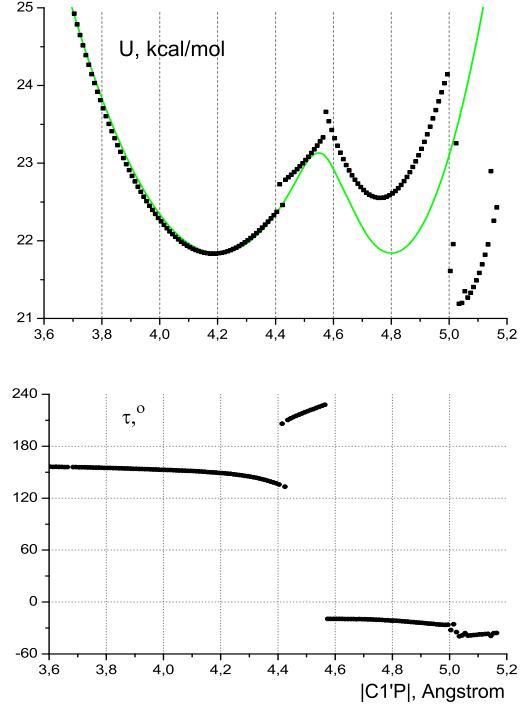


FIG. 18. Potential of interaction between the grains $C1'$ and $P(2)$, obtained by method of "relaxation" (see the beginning of section IID). On the top: dependence of the energy of the "relaxed" fragment on the distance $|C1'P(2)|$. The solid smooth curve is the potential used in the sugar CG model. On the bottom: dependence of the pseudorotational angle τ on $|C1'P(2)|$. At the distances in the area of the left minimum of the potential the ribose is in the south region (B-DNA), and in the area of the right minimum - in the north region (A-DNA). In the transition through the barrier, the pucker goes through the west region.

VIII. APPENDIX B: POTENTIALS OF INTERACTIONS BETWEEN IONS AND BETWEEN IONS AND DNA GRAINS: DERIVATION AND PARAMETERS

The parameters of the effective (solvent-mediated) potentials of interaction (3) for the pairs Cl^-Na^+ and Cl^-Cl^- (adopted from work⁴⁵) are listed in table XI. The parameters of the potential of interaction of Cl^- ions with phosphate grains Cl^-P^- (from article⁴⁴) are given in table X, together with the parameters for Na^+P^- interactions.

We derived the potentials of interaction between ions and grains on bases B_j from Na^+Na^+ , Na^+Cl^- and Cl^-Cl^- potentials obtained in⁴⁵. The procedure, which we assume to give qualitatively correct shape of the potential curves, was as follows. Radial distribution function (rdf) for any two charged particles in a solvent has two or three pronounced local maxima. The first maximum corresponds to the direct contact of ions. It is absent for the like-charged particles. The second maxi-

TABLE VIII. "Valence" and two "torsion" angles in the backbone (...C3'-P-C3'-P...) of a DNA strand. In crystallographic (GLACTONE³⁰) A- and B-DNA forms *A-Gl* *B-Gl*, as well as in MD simulations the values of these angles are close. The order of atoms in the notations of the angles is their order along the chain direction (see fig. 5).

ϕ_{A-Gl}		A
<hr/>		
$\angle C3'PC3'$,		
$\phi, ^0$	110.6	110 \pm 14
$K_\phi,$		1.2 \pm 0.5
$10^{-2} \frac{kcal}{mol \cdot deg^2}$		
<hr/>		
$\angle C3'PC3'P,$		
$\phi, ^0$	168	173 \pm 32
$K_\phi,$		0.23 \pm 0.05
$10^{-2} \frac{kcal}{mol \cdot deg^2}$		
<hr/>		
$\angle PC3'PC3',$		
$\phi, ^0$	215	217 \pm 30
$K_\phi,$		0.28 \pm 0.15
$10^{-2} \frac{kcal}{mol \cdot deg^2}$		
<hr/>		
ϕ_{B-Gl}		B
<hr/>		
$\angle C3'PC3',$		
$\phi, ^0$	130.2 ⁰	104 \pm 13
$K_\phi,$		1.4 \pm 0.6
$10^{-2} \frac{kcal}{mol \cdot deg^2}$		
<hr/>		
$\angle C3'PC3'P,$		
$\phi, ^0$	158	179 \pm 31
$K_\phi,$		0.25 \pm 0.09
$10^{-2} \frac{kcal}{mol \cdot deg^2}$		
<hr/>		
$\angle PC3'PC3',$		
$\phi, ^0$	224	211 \pm 44 (90%) // 135 \pm 27 (10%)
$K_\phi,$		0.12 \pm 0.04 // 0.33 \pm 0.11
$10^{-2} \frac{kcal}{mol \cdot deg^2}$		
<hr/>		

imum is at the distance between the particles across one solvent shell, the third maximum is behind the second solvent shell. We supposed that the position of the first maximum mainly depends on the radii of interacting particles; while the position of the second and the third maxima - on the properties of solvent molecules (size, shape and dipole moment).

Therefore, for every unlike-charged pair ($Cl^- - B_j^+$ or $Na^+ - B_j^-$) we set the location of the first minimum of the effective potential as the sum of the radius of an ion (1.8Å for Cl^- and 1Å for Na^+) and the radius of the grain B_j . For like-charged pairs ($Cl^- - B_j^-$ or $Na^+ - B_j^+$), one should add the thickness of solvation shell to this value. For $Na^+ - Na^+$ and $Cl^- - Cl^-$ interactions it equals about 1.6Å⁴⁵, and we used this value for all our effective potentials of interactions between ions and grains of bases. The second and the third minima of the potentials we put at 2.3Å and 4.3Å from the first minimum: at the distances at which they are in all three potentials of interactions from⁴⁵. For interactions $Na^+ - B_j^-$ we took the heights of the maxima and the depths of the minima relative to the Coulomb asymptotics the same as in the potential for $Na^+ - Cl^-$, and for interactions $Na^+ - B_j^+$ - the same as in the potential for $Na^+ - Na^+$. We also

TABLE IX. "Valence" angles determining the direction of the glycosidic bond relative to the sugar-phosphate backbone in the sugar CG model C3'-C1'-N and P-C1'-N; "torsion" angles for base pairs openings C3'-P-C3'-C1' and C1'-C3'-P-C3'; and the angle of rotation of base around the glycosidic bond in crystallographic (GLACTONE³⁰) A- and B-DNA forms *A-Gl* and *B-Gl*, as well as in MD simulations. The order of atoms in the notation of the angles is their order along the chain direction (see fig. 5).

ϕ_{A-Gl}		A
<hr/>		
$\angle C3'C1'N(1,9),$		
$\phi, ^0$	110.7	112 \pm 3 (65%) // 145 \pm 4 (35%)
$K_\phi, 10^{-2} \frac{kcal}{mol \cdot deg^2}$		2.5 \pm 0.7 // 2 \pm 1
<hr/>		
$\angle PC1'N(1,9),$		
$\phi, ^0$	83.6	84 \pm 10 (77%) // 104 \pm 15 (23%)
$K_\phi, 10^{-2} \frac{kcal}{mol \cdot deg^2}$		2.4 \pm 0.24 // 1.1 \pm 0.1
<hr/>		
$\angle C3'PC3'C1',$		
$\phi, ^0$	8.9	4 \pm 23 (91%) // 31 \pm 13 (9%)
$K_\phi, 10^{-2} \frac{kcal}{mol \cdot deg^2}$		0.44 \pm 0.2 // 1.4 \pm 1
<hr/>		
$\angle C1'C3'PC3',$		
$\phi, ^0$	7	13 \pm 34
$K_\phi, 10^{-2} \frac{kcal}{mol \cdot deg^2}$		0.2 \pm 0.1
<hr/>		
$\angle C3'C1'-$		
$-N(1,9)C(6,8),$		
$\phi, ^0$	-51.4	-32 \pm 9
$K_\phi, 10^{-2} \frac{kcal}{mol \cdot deg^2}$		3.2 \pm 0.1
<hr/>		
ϕ_{B-Gl}		B
<hr/>		
$\angle C3'C1'N(1,9),$		
$\phi, ^0$	141.5	146 \pm 13
$K_\phi, 10^{-2} \frac{kcal}{mol \cdot deg^2}$		1.46 \pm 0.6
<hr/>		
$\angle PC1'N(1,9),$		
$\phi, ^0$	87	88 \pm 12 (32%) // 105 \pm 14 (68%)
$K_\phi, 10^{-2} \frac{kcal}{mol \cdot deg^2}$		1.7 \pm 0.6 // 1.2 \pm 0.35
<hr/>		
$\angle C3'PC3'C1',$		
$\phi, ^0$	49	3 \pm 28 (80%) // 22 \pm 19 (20%)
$K_\phi, 10^{-2} \frac{kcal}{mol \cdot deg^2}$		0.3 \pm 0.1 // 0.64 \pm 0.2
<hr/>		
$\angle C1'C3'PC3',$		
$\phi, ^0$	-26	11 \pm 33
$K_\phi, 10^{-2} \frac{kcal}{mol \cdot deg^2}$		0.2 \pm 0.1
<hr/>		
$\angle C3'C1'-$		
$-N(1,9)C(6,8),$		
$\phi, ^0$	-1.5	-27 \pm 34
$K_\phi, 10^{-2} \frac{kcal}{mol \cdot deg^2}$		0.22 \pm 0.06
<hr/>		

accepted that the energy of interaction between the particles at the distance less by 0.5Å than the position of the first minimum is 3kT. Analogously, the potentials for the pairs $Cl^- - B_j^-$ and $Cl^- - B_j^+$ were patterned after the potentials between the pairs $Cl^- - Cl^-$ and $Cl^- - Na^+$.

All the grains put on the groups NH_2 (B_2 on C, B_2 on A, B_3 on G) are positively charged (see table II). We accepted for their radii the value $r_N = 1.6Å$, $r_N = r_{N-H} + r_H$, where $r_{N-H} = 1Å$ - the distance between the centers of nitrogen and hydrogen, and $r_H = 0.6Å$ - van der Waals radius of hydrogen in the AMBER force field.

Three of four grains put on the oxygen atoms (B_3 on C,

TABLE X. Parameters A , D_k , C_k , R_k for potentials of interaction (3) between a sodium ion and a phosphate grain $\text{Na}^+\text{-P}^-$ and between a chlorine ion and a phosphate grain $\text{Cl}^-\text{-P}^-$ in the sugar CG DNA model.

parameter	dimension	$\text{Na}^+\text{-P}^-$	$\text{Cl}^-\text{-P}^-$
A	$\text{kcal/mol}\cdot\text{\AA}^{12}$	$8.50 \cdot 10^5$	$10.2 \cdot 10^7$
D_1		-1.25	-0.05
D_2		1.54	0.54
D_3	kcal/mol	-0.73	-0.02
D_4		0.53	0.25
D_5		-0.38	0
C_1		0.92	2.9
C_2		5.00	2.0
C_3	\AA^{-2}	0.75	0.5
C_4		5.50	0.7
C_5		0.90	0
R_1		3.65	5.4
R_2		4.18	6.7
R_3	\AA	5.86	8.6
R_4		6.70	8.9
R_5		7.97	0
ε		80	80

TABLE XI. Parameters A , D_k , C_k , R_k for potentials of interaction (3) between two sodium ions $\text{Na}^+\text{-Na}^+$ and between a sodium ion and a chlorine ion $\text{Na}^+\text{-Cl}^-$ and between two chlorine ions $\text{Cl}^-\text{-Cl}^-$ in the sugar CG DNA model.

	dimension	$\text{Na}^+\text{-Na}^+$	$\text{Na}^+\text{-Cl}^-$	$\text{Cl}^-\text{-Cl}^-$
A	$\frac{\text{kcal}}{\text{mol}} \cdot \text{\AA}^{12}$	$15.0 \cdot 10^5$	$2.2 \cdot 10^5$	$4.0 \cdot 10^7$
D_1		-0.62	-1.36	-0.52
D_2		0.29	1.87	0.29
D_3	kcal/mol	-0.55	-0.27	-0.07
D_4		0.16	0.276	0.06
D_5		-0.25	-0.073	-0.022
C_1		1.4	5.0	3.0
C_2		4.0	2.0	4.0
C_3	\AA^{-2}	0.7	1.5	3.5
C_4		5.5	5.5	3.0
C_5		1.5	5.0	3.0
R_1		3.40	2.80	5.00
R_2		4.75	3.62	6.35
R_3	\AA	6.20	5.20	7.60
R_4		7.15	6.00	8.50
R_5		8.47	6.80	9.70
ε		80	80	80

B_2 and B_3 on T) are negatively charged, and we accepted for their radii the value 1.66\AA - van der Waals radius of oxygen in the AMBER force field. The fourth grain on an oxygen, B_2 (G), carries a small positive charge because the dipole moment of base G has component along the axis C6-C8. Actually, the partial charge on atom O6 is negative, $(-0.57e)$ in AMBER force field.

As a matter of fact, the main difference between the base pairs AT and GC is that the atoms of G looking into the major groove carry large negative charge, and

the atoms of C - large positive charge. Namely (see fig. 1), the atoms N_7 and O_6 of G attract Na^+ ions into the major groove in A-DNA, and stabilize them in this groove. Correspondingly, chlorine ions near DNA can be found beside atom N_4 on C (more exactly, beside hydrogen atoms connected with atoms N_4 and C_5). Contrary to this picture, bases A and T have almost zero component of electric dipole moment orthogonal to the axis C6-C8.

To model the above described feature of base G, we set the location of the first minimum of the potential for $\text{Na}^+\text{-B}_2(\text{O}_6)$ on G at 2.5\AA , which corresponds to the radius of the grain 1.5\AA , and to the absence of the solvation shell (sodium ions can come up close to these grains as if they were negatively charged). The radius of the negatively charged grain $B_1(\text{C}_8)$ on G for interaction with sodium ions was taken to be 1.3\AA , the depth of the first minimum was shifted down by $1.3kT$, and the depth of the second minimum - by $0.4 kT$. To not prevent the sodium ions from dwelling in the major groove, the radii of the grains B_1 on A (C_8) and B_1 on T (C_7) were chosen to be 1.7\AA and 1.5\AA correspondingly. The above mentioned small radii of these three grains are maximum values at which sodium ions keep inside the major groove in A-DNA.

For the grain $B_1(\text{C}_6)$ on C with large positive charge we set the radius $r_C = 2.5\text{\AA} = r_{C-H} + r_{H_4}$, where $r_{C-H} = 1\text{\AA}$ - the distance between the centers of carbon and hydrogen, and $r_{H_4} = 1.4\text{\AA}$ - van der Waals radius of hydrogen in the AMBER force field. The same value, 2.5\AA , was taken for the radius of the grain $B_3(\text{C}_2)$ on A, as well as for all the grains put on carbon atoms (B_1 on A, T, C, G and B_3 on A) in their potentials of interactions with chlorine ions.

Parameters $\{A, D_k, C_k, R_k\}$ of so obtained potentials (3) are listed in tables XII, XIII, XIV, XV. The plots of some effective potentials used in the CG DNA model are shown in figures 19 and 20.

TABLE XII. Parameters A , D_k , C_k , R_k for potentials of interaction (3) between a sodium ion and base grains Na^+-B_j in the sugar CG DNA model. The case of Adenine and Thymine.

parameter	dimension	Na^+-B_1	Na^+-B_2	Na^+-B_3
Adenine				
$\sqrt[12]{A}$	$\sqrt[12]{\text{kcal/mol}\text{\AA}}$	2.43	4.0	3.256
D_1		-1.0	-1.237	1.11
D_2		1.6	0.307	2.1
D_3	kcal/mol	-0.4	-0.3	-0.298
D_4		0.2	0.115	0.13
D_5		-0.1	-0.08	-0.0895
C_1		2	2	2.8
C_2		4	4.5	4
C_3	\AA^{-2}	2	2	2
C_4		7	7	7
C_5		2	2	2
R_1		2.52	4.05	3.5
R_2		3.6	5.27	4.7
R_3	\AA	4.9	6.53	5.8
R_4		6.2	7.53	6.9
R_5		7.4	8.53	7.8
Thymine				
$\sqrt[12]{A}$	$\sqrt[12]{\text{kcal/mol}\text{\AA}}$	3.86	2.366	2.366
D_1		-1.4	-1.0	-1.0
D_2		0.483	2.19	2.19
D_3	kcal/mol	-0.5	-0.298	-0.298
D_4		0.104	0.132	0.132
D_5		-0.073	-0.0895	-0.0895
C_1		3	3.42	3.42
C_2		5	4.5	4.5
C_3	\AA^{-2}	1.5	2.0	2.0
C_4		5	7	7
C_5		3	2	2
R_1		3.9	2.66	2.66
R_2		4.8	3.45	3.45
R_3	\AA	5.2	4.96	4.96
R_4		6.46	6.1	6.1
R_5		7.4	6.96	6.96
ϵ		80	80	80

TABLE XIII. Parameters A , D_k , C_k , R_k for potentials of interaction (3) between a sodium ion and base grains Na^+-B_j in the sugar CG DNA model. The case of Guanine and Cytosine.

parameter	dimension	Na^+-B_1	Na^+-B_2	Na^+-B_3
Guanine				
$\sqrt[12]{A}$	$\sqrt[12]{\text{kcal/mol}\text{\AA}}$	1.78	2.187	3.97
D_1		-0.85	-0.75	-1.18
D_2		2.149	1.5	0.304
D_3	kcal/mol	-0.55	-0.298	-0.243
D_4		0.2	0.132	0.114
D_5		-0.3	-0.22	-0.073
C_1		3	3.4	3.6
C_2		4.5	4.5	4.5
C_3	\AA^{-2}	2	2	2
C_4		7	7	5
C_5		2	2	3
R_1		2.4	2.5	4.06
R_2		3.29	3.29	5.27
R_3	\AA	4.8	4.6	6.53
R_4		5.94	5.94	7.53
R_5		6.9	6.8	8.53
Cytosine				
$\sqrt[12]{A}$	$\sqrt[12]{\text{kcal/mol}\text{\AA}}$	4.92	4.0	2.366
D_1		-1.7	-1.4	-0.6
D_2		0.283	0.31	2.147
D_3	kcal/mol	-0.5	-0.41	-0.298
D_4		0.104	0.104	0.132
D_5		-0.21	-0.17	-0.0895
C_1		1.5	1.5	3.42
C_2		5.5	4.5	4.5
C_3	\AA^{-2}	2.0	1.6	2.0
C_4		5.0	5.0	7.0
C_5		3.0	3.0	2.0
R_1		4.94	4.03	2.66
R_2		6.2	5.07	3.45
R_3	\AA	7.4	6.23	4.96
R_4		8.46	7.53	6.1
R_5		9.4	8.53	6.96
ϵ		80	80	80

TABLE XIV. Parameters A , D_k , C_k , R_k for potentials of interaction (3) between a chlorine ion and base grains Cl^- - B_j in the sugar CG DNA model. The case of Adenine and Thymine.

parameter	dimension	Cl^- - B_1	Cl^- - B_2	Cl^- - B_3
Adenine				
$\sqrt[12]{A}$	$\sqrt[12]{\text{kcal/mol}\text{\AA}}$	5.7	3.2	5.7
D_1		-1.5	-1.11	-1.5
D_2	kcal/mol	0.29	2.1	0.29
D_3		-0.245	-0.298	-0.245
D_4		0.105	0.13	0.105
D_5		-0.07	-0.0895	-0.073
C_1		3	2.8	3
C_2		4	4	4
C_3	\AA^{-2}	2	2	2
C_4		4	7	4
C_5		3	2	3
R_1		5.65	3.3	5.81
R_2		6.96	4.59	6.96
R_3	\AA	8.11	5.74	8.11
R_4		9.11	6.74	9.11
R_5		10.11	7.74	10.11
Thymine				
$\sqrt[12]{A}$	$\sqrt[12]{\text{kcal/mol}\text{\AA}}$	4.1	4.79	4.79
D_1		-1.3	-1.39	-1.39
D_2	kcal/mol	2.1	0.317	0.317
D_3		-0.298	-0.245	-0.245
D_4		0.13	0.105	0.105
D_5		-0.0895	-0.070	-0.070
C_1		2.8	3	3
C_2		4	4	4
C_3	\AA^{-2}	2	2	2
C_4		7	4	4
C_5		2	3	3
R_1		4.12	4.76	4.76
R_2		5.46	6.12	6.12
R_3	\AA	6.61	7.27	7.27
R_4		7.61	8.27	8.27
R_5		8.61	9.27	9.27
ε		80	80	80

TABLE XV. Parameters A , D_k , C_k , R_k for potentials of interaction (3) between a chlorine ion and base grains Cl^- - B_j in the sugar CG DNA model. The case of Guanine and Cytosine.

parameter	dimension	Cl^- - B_1	Cl^- - B_2	Cl^- - B_3
Guanine				
$\sqrt[12]{A}$	$\sqrt[12]{\text{kcal/mol}\text{\AA}}$	4.6	3.2	3.2
D_1		-1.36	-1.11	-1.11
D_2	kcal/mol	0.317	2.1	2.10
D_3		-0.245	-0.298	-0.298
D_4		0.105	0.13	0.130
D_5		-0.070	-0.0895	-0.0895
C_1		3	2.8	2.8
C_2		4	4	4
C_3	\AA^{-2}	2	2	2
C_4		4	7	7
C_5		3	2	2
R_1		4.6	3.3	3.3
R_2		5.96	4.62	4.59
R_3	\AA	7.11	5.77	5.74
R_4		8.11	6.9	6.74
R_5		9.11	7.77	7.74
Cytosine				
$\sqrt[12]{A}$	$\sqrt[12]{\text{kcal/mol}\text{\AA}}$	4.1	3.2	4.79
D_1		-1.3	-1.11	-1.39
D_2	kcal/mol	2.1	2.1	0.317
D_3		-0.298	-0.298	-0.245
D_4		0.13	0.13	0.105
D_5		-0.0895	-0.0895	-0.070
C_1		2.8	2.8	3
C_2		4	4	4
C_3	\AA^{-2}	2	2	2
C_4		7	7	4
C_5		2	2	3
R_1		4.12	3.3	4.76
R_2		5.46	4.59	6.12
R_3	\AA	6.61	5.74	7.27
R_4		7.61	6.74	8.27
R_5		8.61	7.74	9.27
ε		80	80	80

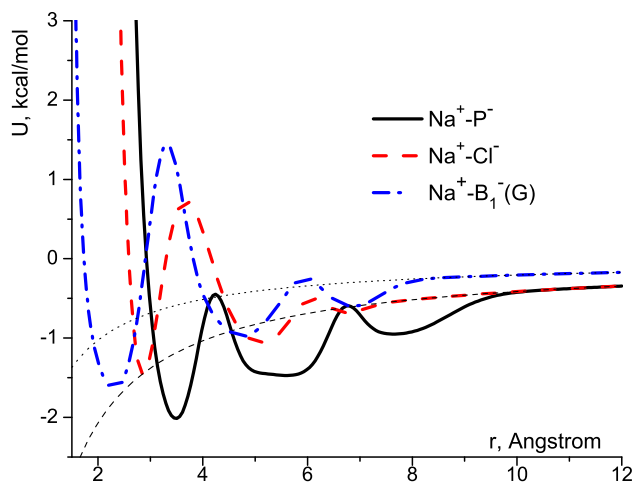


FIG. 19. Effective potentials of attraction between ions and charged grains in the sugar CG DNA model. The parameters of the potentials are listed in tables X and XII. Thin dashed and dotted curves correspond to the Coulombic interaction between the charges (the last term in equation (3)).

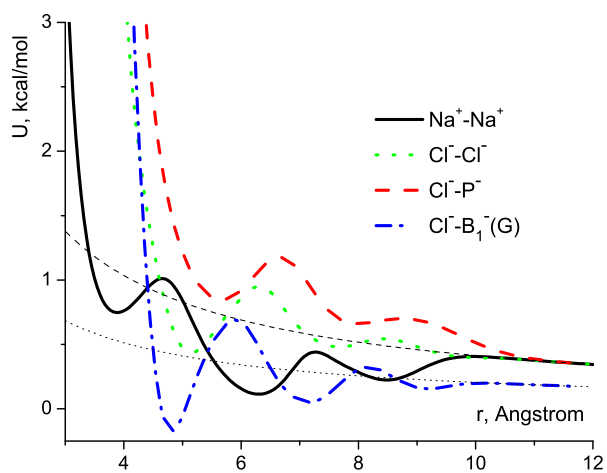


FIG. 20. Effective potentials of repulsion between ions and charged grains in the sugar CG DNA model. The parameters of the potentials are listed in tables X and XII. Thin dashed and dotted curves correspond to the Coulombic interaction between the charges (the last term in equation (3)).

- ¹P. Varnai, D. Djuranovic, R. Lavery, and B. Hartmann, *NAR* **30**, 5398 (2002).
- ²B. Hartmann, D. Piazzola, and R. Lavery, *NAR* **21**, 561 (1993).
- ³A. Lebrun and R. Lavery, *Biopolymers* **49**, 341 (1999).
- ⁴X.-J. Lu, Z. Shakked, and W. Olson, *J. of Mol. Biology* **300**, 819 (2000).
- ⁵S. Mohr, N. Sokolov, C. He, and P. Setlow, *PNAS* **88**, 77 (1991).
- ⁶S. Arnott, *Trends in Biochem. Sci.* **31**, 349 (2006).
- ⁷V. Ivanov, L. Minchenkova, A. Schyolkina, and A. Poletayev, *Biopolymers* **12**, 89 (1973).
- ⁸Y. Nishimura, C. Torigoe, and M. Tsuboi, *NAR* **14**, 2737 (1986).
- ⁹V. Ivanov and D. Krylov, "A-DNA in solution as studied by diverse approaches," in *DNA Structures Part A: Synthesis and Physical Analysis of DNA*, Meth. in Enzymology, Vol. 211 (Elsevier, 1992) pp. 111-127.
- ¹⁰H. Karimi-Varzaneh and F. Muller-Plathe, *Topics in current chemistry* **307**, 295 (2012).
- ¹¹S. Takada, *Current opinion in struct. biol.* **22**, 130 (2012).
- ¹²D. Potoyan, A. Savelyev, and G. Papoian, *WIREs: Comp. Mol. Sci.* **3**, 69 (2013).
- ¹³A. Mazur, *J. Phys. Chem. B* **113**, 2077 (2009).
- ¹⁴N. Becker and R. Everaers, *Phys. Rev. E* **76**, 021923 (2007).
- ¹⁵J. Kim, J. Jeon, and W. Sung, *J. of Chem. Phys.* **128**, 055101 (2008).
- ¹⁶T. Knotts IV, N. Rathore, D. Schwartz, and J. de Pablo, *J. of Chem. Phys.* **126**, 084901 (2007).
- ¹⁷N. Kovaleva, L. Manevich, A. Musienko, and A. Savin, *Pol. Sci. Series A* **51**, 833 (2009).
- ¹⁸A. Andrews, J. Rottler, and S. Plotkin, *J. of Chem. Phys.* **132**, 035105 (2010).
- ¹⁹I. Kikot, E. Zubova, M. Mazo, N. Kovaleva, and L. Manevitch, *Proceedings of the XXXVIII Summer School Conference "Advanced Problems in Mechanics"*, APM-2010, https://doi.org/10.1007/978-3-70-010010-1_299 (2010).
- ²⁰I. Kikot, A. Savin, E. Zubova, M. Mazo, E. Gusarova, L. Manevitch, and A. Onufriev, *Biophysics* **56**, 387 (2011).
- ²¹J. Srinivasan, M. Trevathan, P. Beroza, and D. Case, *Theor. Chem. Acc.* **101**, 426 (1999).
- ²²A. Savin, M. Mazo, I. Kikot, L. Manevitch, and A. Onufriev, *Phys. Rev. B* **83**, 245406 (2011).
- ²³A. Savin, I. Kikot, M. Mazo, and A. Onufriev, *PNAS* **110**, 2816 (2013).
- ²⁴J. Wang, P. Cieplak, and P. Kollman, *J. of Comp. Chem.* **21**, 1049 (2000).
- ²⁵J. Sponer, P. Jurecka, I. Marchan, F. Luque, M. Orozco, and P. Hobza, *Chem. Eur. J.* **12**, 2854 (2006).
- ²⁶S. Neidle, *Principles of Nucleic Acid Structure* (Elsevier Academic Press, 2008).
- ²⁷M. Feig and B. Pettitt, *Biophys. J.* **77**, 1769 (1999).
- ²⁸A. Gelbin, B. Schneider, L. Clowney, S.-H. Hsieh, W. Olson, and H. Berman, *J. of the Am. Chem. Soc.* **118**, 519 (1996).
- ²⁹N. Bruant, D. Flatters, R. Lavery, and D. Genest, *Biophys. J.* **77**, 2366 (1999).
- ³⁰"ideal" DNA structures constructed by GLACTONE program according to a
- ³¹D. Sprous, M. A. Young, and D. L. Beveridge, *J. Phys. Chem. B* **102**, 4658 (1998).
- ³²A. K. Mazur, *J. Am. Chem. Soc.* **125**, 7849 (2003).
- ³³L. Yang and B. Pettitt, *J. Phys. Chem.* **100**, 2564 (1996).
- ³⁴W. Tschop, K. Kremer, J. Batoulis, T. Burger, and O. Hahn, *Acta Polym.* **49**, 61 (1998).
- ³⁵A. Perez, I. Marchan, D. Svozil, J. Sponer, T. Cheatham III, C. Laughton, and M. Orozco, *Biophys. J.* **92**, 3817 (2007).
- ³⁶N. Foloppe, L. Nilsson, and A. MacKerell, *Biopolymers* **61**, 61 (2001).
- ³⁷T. Cheatham III, M. Crowley, T. Fox, and P. Kollman, *PNAS* **94**, 9626 (1997).
- ³⁸B. Jayaram, D. Sprous, M. A. Young, and D. L. Beveridge, *J. Am. Chem. Soc.* **120**, 10629 (1998).
- ³⁹J. Chocholousova and M. Feig, *J. Phys. Chem. B* **110**, 17240 (2006).
- ⁴⁰L. Wang, B. Hingerty, A. Srinivasan, W. Olson, and S. Broyde, *Biophys. J.* **83**, 382 (2002).
- ⁴¹J. Mazur and R. Jernigan, *Biopolymers* **31**, 1615 (1991).
- ⁴²G. Freeman, D. Hinckley, and J. de Pablo, *J. of Chem. Phys.* **135**, 165104 (2011).
- ⁴³B. Hingerty, R. Ritchie, T. Ferrell, and J. Turner, *Biopolymers* **24**, 427 (1985).
- ⁴⁴A. Lyubartsev and A. Laaksonen, *J. of Chem. Phys.* **111**, 11207 (1999).
- ⁴⁵A. Lyubartsev and S. Marčelja, *Phys. Rev. E* **65**, 041202 (2002).
- ⁴⁶B. Hess, C. Holm, and N. van der Vegt, *Phys. Rev. Lett.* **96**, 147801 (2006).
- ⁴⁷A. Savelyev and G. Papoian, *J. of Phys. Chem. B* **113**, 7785 (2009).
- ⁴⁸G. Smith and L. Ding, *J. of Chem. Phys.* **100**, 3757 (1994).
- ⁴⁹A. Lyubartsev and A. Laaksonen, *J. of Biomol. Struct. and Dyn.* **16**, 579 (1998).
- ⁵⁰N. Prabhu, M. Panda, Q. Yang, and K. Sharp, *J. of Comp. Chem.* **29**, 1113 (2008).
- ⁵¹T. Gaillard and D. Case, *J. of Chem. Theory and Computaion* **7**, 3181 (2011).
- ⁵²J.-W. Shen, C. Li, N. van der Vegt, and C. Peter, *J. of Chem. Theory and Comp.* **7**, 1916 (2011).
- ⁵³A. Noy, I. Soteras, F. Luque, and M. Orozco, *Phys. Chem. Chem. Phys.* **11**, 10596 (2009).
- ⁵⁴I. Joung and T. Cheatham III, *J. Phys. Chem. B* **112**, 90209041 (2008).
- ⁵⁵G. Giambaşu, T. Luchko, D. Herschlag, D. York, and D. Case, *Biophys. J.* **106**, 883 (2015).
- ⁵⁶M. Feig and B. Pettitt, *J. Phys. Chem. B* **101**, 7361 (1997).
- ⁵⁷A. Noy, A. Perez, C. Laughton, and M. Orozco, *NAR* **35**, 3330 (2007).
- ⁵⁸U. Priyakumar and A. MacKerell, *Chem. Rev.* **106**, 489 (2006).